Waveguide Chirped-Pulse Fourier Transform Microwave Spectra of Small Alkylthiols

By

Bri Gordon

A Thesis

Submitted to the Division of Natural Sciences
New College of Florida
in partial fulfillment of the requirements for the degree
Bachelor of Arts in Chemistry
Under the sponsorship of Dr. Steven T. Shipman

Sarasota, Florida
May, 2013

Acknowledgements

I would like to thank my committee, Dr. Shipman, Dr. Sherman, and Dr. Scudder as well as my lab mates from the past and present, Ben Rooks, Christian Metzgar, Maria Phillips, and Ian Finneran. Thank you and good look carrying on our work: Morgan McCabe, Erin Kent, Sophie Lang, Sam Weldon, Anne Emig, Zach Decker, Michael Davis, and Lauren Bernier. Special thanks to my family and best friends, Charlotte Gray, Jessie Ploss, and Paris Tressler for your support and friendship.

Table of Contents

Table of Figures

Table of Tables

Waveguide Chirped-Pulse Fourier Transform Microwave Spectra of Small Alkylthiols

Bri Gordon
New College of Florida, 2013

Abstract

The microwave spectra of three small alkylthiols (ethanethiol, 1-propanethiol, and 2-propanethiol) were measured from 8.7—26.5 GHz with waveguide chirped-pulse Fourier transform microwave spectroscopy (CP-FTMW) at ~250 K. All three of these alkylthiols can be either trans or gauche with respect to the C-S bond, and both conformers are present in reasonable abundance for each molecule. In fact, transitions from the 34S isotopically-substituted species are also easily seen in natural abundance. These molecules have been previously studied but our spectrometer is significantly more sensitive than prior instruments and we have been able to extend these prior fits to substantially higher values of the J rotational constant.

Steven T. Shipman

Division of Natural Sciences

1) Introduction

Microwave spectroscopy studies the rotational spectra of small gas phase molecules with permanent dipoles. Different regions of the electromagnetic spectrum interact with molecules in various ways depending on wavelength. UV and visible light are associated with electronic transitions, infrared light is associated with vibrational transitions, and microwaves are associated with rotational transitions.

Unlike some other forms of molecular spectroscopy, in rotational spectroscopy, peak positions are not uniquely correlated with structural features of the molecule. The rotational inertia changes with small variations in bond length, dihedral angle, and mass. Therefore, each conformer, vibrational state, and isotopomer populated by a molecule has a unique spectrum within the measured signal. Because of this, microwave spectra are like fingerprints that can be used to identify individual molecules in complex mixtures.

With microwave spectroscopy we measure the change in rotational energy. The frequency of the transition gives the energy difference between the rotational levels involved in that transition, but does not tell which levels those are. This information can only be obtained by fitting the spectrum to determine rotational constants. Fitting microwave spectra is a challenging process that will be discussed later in this thesis.

While determining rotational constants from experimental data is challenging, it is simple to predict a spectrum from refined rotational constants.

Furthermore, rotational spectra can be observed from 1 GHz to 1 THz. The spectrum in the THz regime is described by the same constants used for the spectrum in the GHz regime. It follows that the constants calculated from the GHz regime can be used to predict spectra in the THz regime. This is particularly important for astrochemistry, which is one of the most important applications of microwave spectroscopy. Astrochemists study the interstellar medium (ISM), which is the matter that exists in between different star systems. Most of the matter in the ISM is in the form of gas and dust which collects to form diffuse clouds and nebulae. Astrochemists can use radio telescopes to collect spectra in the THz regime from the ISM but it is impossible to identify what molecules are present without referencing laboratory constants. Almost all of the molecules that have been discovered in the interstellar medium have been identified by their rotational spectra.

One of the major focuses of astrochemistry lies in determining the ages of astronomical bodies. One way astrochemists hope to do this is by using the relative abundances of different molecules as molecular clocks.[1][2] The sulfur bearing molecules H_2S, SO, and SO_2 are of particular interest as molecular clocks. According to Wakelam *et al.*, "the identity of the major reservoir of sulfur in cold molecular dust clouds is a long standing and unresolved problem, for the sum of the detectable S-bearing molecules is only a very small fraction of the elemental S abundance."[1]

In order to better determine sulfur abundance in the ISM, we need to be able to detect more S-bearing molecules. Many of these molecules have previously been undetectable due to the hardware limitations of the radio telescopes used to observe the ISM. However, the recently completed Atacama Large Millimeter Array

(ALMA) will dramatically increase the number of detectable molecules. ALMA is an astronomical interferometer of radio telescopes in the Atacama desert on the northern Chile Chajnantor plateau at 5000 meters altitude. Not only are the altitude and dry climate of its location ideal for observations, but ALMA is both the largest and most advanced radio telescope ever built. [3] This means that ALMA's spectral surveys will have significantly better resolution and signal-to-noise than previous instruments and molecules that were previously in the noise will now be detectable. However, laboratory constants are still needed in order to identify these molecules. With the number of detectable molecules increasing, it is critical that we generate and improve laboratory constants of more complicated species so that they can be identified.

Methanethiol (methyl mercaptan) has been found in the interstellar medium,[4] but thiols with longer alkyl chains have not yet been detected. With ALMA's enhanced sensitivity, it is reasonable to expect that these larger molecules may soon be found. To help guide searches for these species, we have collected and assigned the rotational spectra of three alkylthiols: ethanethiol (EtSH), 1-propanethiol (1-PrSH), and 2-propanethiol (2-PrSH). Collecting their spectra near 250 K allows us to identify and assign transitions at fairly high values of the J quantum number; this provides us with accurate spectroscopic constants to improve spectral predictions at millimeter- and submillimeter-wave frequencies.

2) Theory of Rotational Spectroscopy

Much of the existing literature on rotational spectroscopy was written with other spectroscopists in mind, rather than as an introductory source. While these are invaluable resources for dealing with advanced problems, there are few resources available that offer a concise explanation of the theory in an approachable way. For this reason, Ian Finneran has written a comprehensive explanation of the theory of rotational spectroscopy in his senior thesis. [5] This has served as the primary introductory instructional material for students in Dr. Shipman's lab for the last three years. What follows is the material relevant to understanding this thesis, using Ian Finneran's thesis as the primary source.

Microwave spectroscopy studies the rotational spectra of molecules. The energy of a rotating molecule is purely kinetic and depends only on the molecule's moments of inertia (I) and angular momentum (J). Since molecules are quantum mechanical systems, their rotational energy levels are quantized, meaning that they can only take on a set of discrete values. It follows that a molecule's total angular momentum is also quantized.

$$E = \frac{1}{2}\left(\frac{J^2}{I}\right) \tag{2.1}$$

The three scalar quantities, J_a, J_b, and J_c, describe the angular momentum along each Cartesian axis. The total angular momentum is the vector sum of these components:

$$J^2 = J_a^2 + J_b^2 + J_c^2 \tag{2.2}$$

The rotation of the molecule depends on the distribution of its moments of inertia. The rotational constants A, B, and C, are used to describe the rotation of the

molecule and are inversely proportional to their respective moments of inertia, such that:

$$A = \frac{\hbar^2}{2I_a} \qquad B = \frac{\hbar^2}{2I_b} \qquad C = \frac{\hbar^2}{2I_c} \tag{2.3}$$

where $I_a \leq I_b \leq I_c$.

It is the convention in microwave spectroscopy to rename the three Cartesian axes as a, b, and c. The axes are labeled so that A is the largest rotational constant (I_A is the smallest moment of inertia) and C is the smallest rotational constant (I_C is the largest moment of inertia). In the notation of rotational spectroscopy, equation 2.1 becomes:

$$E = \frac{1}{2}\left(\frac{J_a^2}{I_a} + \frac{J_b^2}{I_b} + \frac{J_c^2}{I_c}\right) = \frac{1}{\hbar^2}(AJ_a^2 + BJ_b^2 + CJ_c^2) \tag{2.4}$$

In a quantum mechanical system, physical states are described as wavefunctions and all measurable parameters (observables) must be associated with operators. An operator acts on the wavefunction, the eigenfunction, to produce a constant value, the eigenvalue. The energy operator is called the Hamiltonian, $\hat{H}$, and it acts on the wavefunction, ψ, to produce the energy eigenvalue, E.

$$\hat{H}\,\psi = E\,\psi \tag{2.5}$$

Since there are no analytical solutions to the Schrodinger equation for systems more complicated than the hydrogen atom, the full Hamiltonian for a rotating molecule cannot be solved exactly. However, the rigid rotor model does have an exact solution, and so its Hamiltonian can be used as an approximation to the full Hamiltonian.

The rigid rotor Hamiltonian is very similar to the energy expression in equation 2.4, except that the angular momentum components act as the operators,

$\hat{J}_a$, $\hat{J}_b$, and $\hat{J}_c$.

$$\hat{H}_{rigid\ rotor} = \frac{1}{\hbar^2}\left(A\hat{J}_a^2 + B\hat{J}_b^2 + C\hat{J}_c^2\right) \tag{2.6}$$

The Hamiltonian is used to calculate energy levels that can be used to predict the actual spectrum. Once these are calculated, we can compare predicted transition frequencies to the experimentally observed frequencies. The model can be adjusted to better match the observed spectrum by assigning transitions to specific frequencies and using those to refine estimates of the parameters of the Hamiltonian. Generating and improving these parameters is one of the main goals of this thesis and of rotational spectroscopy as a whole. Doing this allows spectroscopists to predict a molecule's rotational spectrum anywhere from 1 GHz to 1 THz, which is vital for identifying molecules in complex mixtures, such as the ISM.

While equation (2.6) provides a starting point, it does not allow us to completely describe the rotation of a molecule. There is a fundamental uncertainty in measuring the three angular momentum components simultaneously because $\hat{J}_a$, $\hat{J}_b$, and $\hat{J}_c$ do not commute. Conversely, the square of the total angular momentum, $\hat{J}^2$, and any one of the three components can be measured simultaneously. Hence, the Hamiltonian can be rearranged in terms of $\hat{J}^2$ and one of the components $\hat{J}_a$, $\hat{J}_b$, or $\hat{J}_c$.

The optimal arrangement of the Hamiltonian depends on the distribution of the moments of inertia. Depending on their symmetries, molecules can be categorized as one of five classes: Spherical ($I_a = I_b = I_c$), Linear ($I_a = 0$, $I_b = I_c$), prolate ($I_a < I_b = I_c$), oblate ($I_a = I_b < I_c$), and asymmetric ($I_a < I_b < I_c$). The first four can be solved exactly and their rearranged Hamiltonians are listed below:

$$\hat{H}_{sperical} = \frac{1}{\hbar^2}\left(A\hat{J}_a^2 + B\hat{J}_b^2 + C\hat{J}_c^2\right) = \frac{A}{\hbar^2}\left(\hat{J}_a^2 + \hat{J}_b^2 + \hat{J}_c^2\right) = \frac{A}{\hbar^2}\hat{J}^2 \tag{2.7}$$

$$\hat{H}_{linear} = \frac{1}{\hbar^2}\left(A\hat{J}_a^2 + B\hat{J}_b^2 + C\hat{J}_c^2\right) = \frac{1}{\hbar^2}\left(B\hat{J}_b^2 + C\hat{J}_c^2\right) = \frac{B}{\hbar^2}\left(\hat{J}_b^2 + \hat{J}_c^2\right) = \frac{B}{\hbar^2}\hat{J}^2 \quad (2.8)$$

$$\hat{H}_{prolate} = \frac{1}{\hbar^2}\left(A\hat{J}_a^2 + B\hat{J}_b^2 + C\hat{J}_c^2\right) = \frac{1}{\hbar^2}\left(A\hat{J}_a^2 + B(\hat{J}_b^2 + \hat{J}_c^2)\right)$$

$$= \frac{1}{\hbar^2}\left(A\hat{J}_a^2 + B(\hat{J}_b^2 - \hat{J}_c^2)\right) = \frac{1}{\hbar^2}\hat{J}_a^2(A - B) + B\hat{J}^2 \quad (2.9)$$

$$\hat{H}_{oblate} = \frac{1}{\hbar^2}\left(A\hat{J}_a^2 + B\hat{J}_b^2 + C\hat{J}_c^2\right) = \frac{1}{\hbar^2}\left(C\hat{J}_a^2 + B(\hat{J}_a^2 + \hat{J}_b^2)\right)$$

$$= \frac{1}{\hbar^2}\left(C\hat{J}_a^2 + B(\hat{J}_a^2 - \hat{J}_b^2)\right) = \frac{1}{\hbar^2}\hat{J}_c^2(C - B) + B\hat{J}^2 \quad (2.10)$$

Oblate and prolate molecules are referred to as symmetric tops and are described by two coordinate systems, the molecular coordinate system and the space-fixed laboratory system. Fortunately, the molecule's orientation relative to the laboratory frame does not affect molecular rotation unless an external field is applied, and so most of the additional parameters from the second coordinate system can be disregarded. Thus, the symmetric rotor wave function can be determined by the quantum numbers J and K, where:

$$K = -J, -J+1, \ldots 0, \ldots, J-1, J \quad (2.11)$$

And the energy eigenvalues can be determined to be: [6]

$$E_{prolate}(J, K_a) = BJ(J+1) + (A-B)K_a^2 \quad (2.12)$$

$$E_{oblate}(J, K_c) = BJ(J+1) + (C-B)K_c^2 \quad (2.13)$$

It can be seen from these equations that the rotational energy is not only dependent on J^2, but also on the projection of *K* onto either the a or c principal axes. This results in 2J+1 rotational energy levels. Additionally, since (A-B) > 0, the

energy of a state at any given J increases with increasing K for the prolate top and decreases for the oblate top. Finally, since K is squared, energy levels with (J, +K) and (J, -K) are degenerate, and so the 2J +1 levels collapse to J+1 distinct levels. [5]

The last class, asymmetric molecules, cannot be solved exactly. However, asymmetric tops can be considered to be hybrids between the prolate and oblate limiting cases, and can be approximated using characteristics from each.[5] The deviation from either limit is quantified by Ray's asymmetry parameter κ, where κ = -1 and κ = 1 correspond to a prolate and an oblate molecule, respectively.

$$\kappa = \frac{2B-A-C}{A-C} \tag{2.14}$$

The hybrid nature of asymmetric molecules means that the energies of +K and -K lose their degeneracies, so there are 2J+1 distinct rotational levels for each value of J. Unfortunately, in asymmetric molecules, the K quantum number no longer has eigenvalues with the same eigenfunctions. The conventional solution is to redefine K to explicitly include contributions from both the prolate and oblate limits, termed K_a and K_c, respectively. The prolate and oblate contributions to the energy levels are demonstrated in Figure 2.1

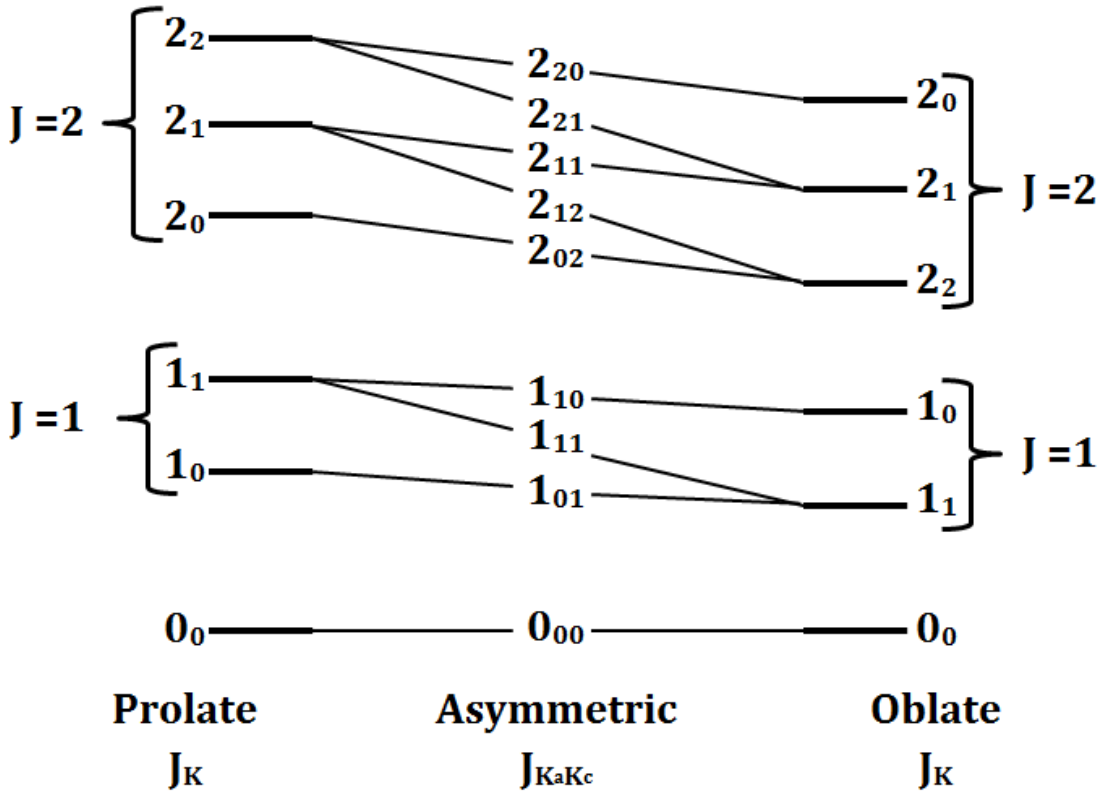

Figure 2.1: The asymmetric top solutions have both prolate and oblate contributions. K_a and K_c refer to the projection of K onto the principal axis in the prolate and oblate cases, respectively. (Adapted from Bernath,[6]pg 191)

Hamiltonians that contain only J^2 and J_c^2 have analytical solutions, but contributions from J_a^2 and J_b^2 render it unsolvable. This is discussed in greater detail in Ian Finneran's senior thesis. [5]

$$\hat{H}_{asymetric} = \hat{H}_{solvable} + \hat{H}_{unsolvable} \tag{2.15}$$

$$\text{where} \quad \hat{H}_{solvble} = \frac{1}{2}(A+C)J^2 - \frac{1}{2}(A-C)J_c^2 \tag{2.16}$$

$$\text{and} \quad \hat{H}_{unsolvable} = \frac{1}{2}(A+C)(\kappa J_a^2 + J_b^2) \tag{2.17}$$

$$\text{Thus,} \quad \hat{H}_{asymmetric} = \frac{1}{2}(A+C)J^2 + \frac{1}{2}(A-C)(J_a^2 + \kappa J_b^2 - J_c^2) \tag{2.18}$$

Since this Hamiltonian cannot be solved exactly, it needs to be approximated and one of the most commonly used approximations is the Watson A-Reduced Hamiltonian because it also addresses deviations from the assumed rigidity by incorporating J- and K-dependent distortion constants. When molecules rotate faster at higher J levels, they display a J-dependent distortion due to centrifugal force. Symmetric and asymmetric tops can have additional K-dependent distortions along one of the axes. [5]

Using this Hamiltonian, we are able to generate a very close match to an experimental spectrum with a relatively small number of parameters. The Watson A-Reduced Hamiltonian up to the quartic constants includes all of the parameters employed in this thesis and can be seen below. The terms of this Hamiltonian are explained in Table 2.1.

$$\hat{H}^{\{A\}}=\hat{H}_r+\hat{H}_d^{\{4\}} \tag{2.19}$$

$$\hat{H}_r=A\hat{J}_a^2+B\hat{J}_b^2+C\hat{J}_c^2 \tag{2.20}$$

$$\hat{H}_d^{\{4\}}=-D_J\hat{J}^4-D_{JK}\hat{J}^2\hat{J}_c^2-D_K\hat{J}_c^4-2d_J\hat{J}^2(\hat{J}_a^2-\hat{J}_b^2)-d_K[\hat{J}_c^2(\hat{J}_a^2-\hat{J}_b^2)+(\hat{J}_a^2-\hat{J}_b^2)\hat{J}_c^2] \tag{2.21}$$

Table 2.1: Terms of the Watson A-Reduced Hamiltonian $\hat{H}^{\{A\}}$ to the quartic constants

Rotational [i] Constants	Symmetric Top [ii] Distortion Constants	Asymmetric Top [iii] Distortion Constants	Operators
A	D_J	d_J	$\hat{J}^2$
B	D_{JK}	d_K	$\hat{J}_a^2$, $\hat{J}_b^2$, $\hat{J}_c^2$
C	D_K		

(i) Dependent on the I_a, I_b, and I_c moments of inertia, (ii) Dependent operators with eigenvalues in the symmetric top basis set, (iii) Dependent on J_a and J_b,
(i), (ii), (iii) are the parameters varied to fit the spectrum

The eigenvalues of this Hamiltonian provide the relative ordering and energies of the rotational energy levels, but the allowed transitions and their intensities are determined by their electric dipoles. A molecule's dipole moment has three components, μ_a, μ_b, and μ_c, along the three principal axes. Since it is the interaction of the dipole moment with the electric field that causes molecules to rotate, the component of the dipole moment along each axis affects the rotational wavefunction along that axis.

The transition dipole moment is proportional to the amount of overlap between the lower and upper state rotational wavefunctions along one of the principal axes and to the projection of the dipole moment along that axis. If there is no overlap, or the dipole moment along the axis of interest is zero, then the transition dipole moment will be zero, and the transition is *forbidden*. But if there is an overlap, and the dipole moment along that axis is non-zero, the transition dipole moment will also be non-zero and the transition will be *allowed*. The selection rules that govern this (shown below) are very stringent and so only a small fraction of the possible transitions are allowed.

$\Delta J = 0, \pm 1 \qquad \Delta K_a = 0, (\pm 2, \pm 4, \ldots) \qquad \Delta K_c = 1, (\pm 3, \pm 5, \ldots) \qquad$ *for* $\mu_a \neq 0$ (2.22)

$\Delta J = 0, \pm 1 \qquad \Delta K_a = 1, (\pm 3, \pm 5, \ldots) \qquad \Delta K_c = 1, (\pm 3, \pm 5, \ldots) \qquad$ *for* $\mu_b \neq 0$ (2.23)

$\Delta J = 0, \pm 1 \qquad \Delta K_a = 1, (\pm 3, \pm 5, \ldots) \qquad \Delta K_c = 0, (\pm 2, \pm 4, \ldots) \qquad$ *for* $\mu_c \neq 0$ (2.24)

The allowed transitions between rotational energy levels are labeled by their dipole moment component and are shown in Figure 2.2 below:

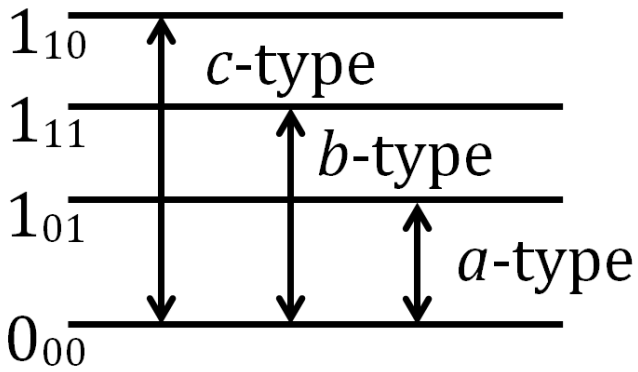

Figure 2.2: *a-*, *b-*, and *c*-type transitions. (Adapted from Bernath,[6] pg 194)

Internal rotation within the molecule can also contribute to and complicate the observed spectrum. *Ab initio* 1D potential energy scans (calculated at the B3LYP/6-311++G(d,p) level of theory in Gaussian 09) were performed on the methyl and thiol dihedrals to calculate if the barriers were low enough for internal rotation. The methyl dihedral scans showed excellent three fold symmetry and were easily fit to a V_3 potential, seen in equation (2.25).

$$E = \left(\frac{V_3}{2}\right)\left(1 - \cos\left(3(\emptyset - 60)\left(\frac{\pi}{180}\right)\right)\right) \qquad (2.25)$$

Thiol dihedral scans were more complicated and an additional V_2 term was added to account for this, giving the equation:

$$E = \left(\frac{V_2}{2}\right)\left(1 - \cos\left(2(\emptyset - 60)\left(\frac{\pi}{180}\right)\right)\right) + \left(\frac{V_3}{2}\right)\left(1 - \cos\left(3(\emptyset - 60)\left(\frac{\pi}{180}\right)\right)\right) \qquad (2.26)$$

These potential energy scans will be discussed further in the following chapters.

The primary program used in our lab is the SPFIT/SPCAT, also known as PICKETT, package of H.M.Pickett.[7] This program uses the Watson A-Reduced Hamiltonian and is well suited for fitting the microwave spectra of many molecules,

including the *trans* conformers of the molecules discussed in this thesis. However, one of the most advantageous attributes of SPFIT/SPCAT is that the Hamiltonian can be extended to include additional parameters for tunneling interactions from a rather extensive built-in library. This feature has been integral to fitting the molecules discussed in this thesis.

3) Experimental

In the Shipman lab, we use a chirped-pulse Fourier transform microwave spectrometer (CP-FTMW) with an 8.7 to 26.5 GHz bandwidth to study the rotational spectra of small gas phase molecules with permanent dipoles. Our instrument is unique in several regards because it combines the chirped-pulse technique developed by the Pate group at the University of Virginia [8] with a waveguide sample cell [9] cooled to ~250 K.

There are three functional units of the spectrometer: the waveform generation circuit, the waveguide sample cell, and the receiver circuit. In the waveform generation circuit, a chirped pulse (linear frequency sweep) from the arbitrary waveform generator (AWG) is upconverted, amplified, and broadcast into the coiled waveguide containing the molecular sample. When the amplified chirped pulse enters the 10 meter coiled WRD-750 waveguide, it polarizes and transiently aligns the molecules so that they rotate in phase with the electric field of the chirped pulse. After the pulse stops, the molecules emit a weak electric field as they continue to rotate in phase until they collide with each other or the waveguide walls, producing a free induction decay (FID). The receiver circuit then collects, amplifies, and downconverts the FID before the signal is digitized by an oscilloscope. The FID is then Fourier transformed to yield the frequency-domain spectrum.

Our instrument has 17.8 GHz of complete coverage between 8.7 and 26.5 GHz. To achieve this bandwidth, we take data in three separate bands, 8.7-13.5 GHz (lower band), 13.5-18.3 GHz, (the middle band), and 18-26.5 GHz (the upper band).

Our microwave spectrometer initially only covered a range from 8.7-18.3 GHz. However, transitions at higher frequencies are significantly more intense in the 18-26 GHz region than those in the 8-18 GHz region (Fig. 3.1).

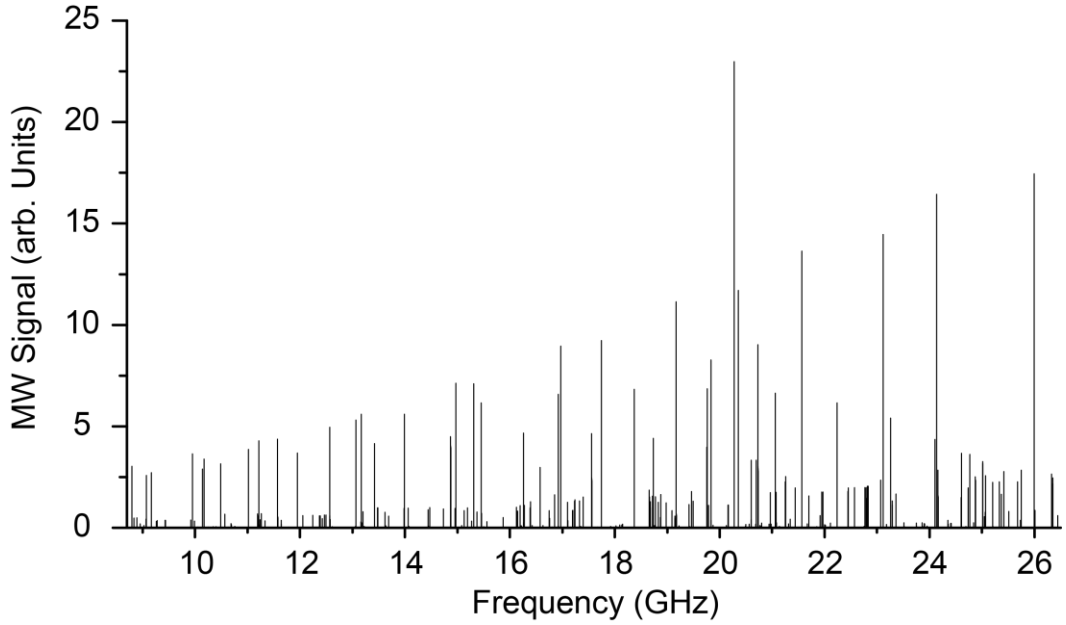

Figure 3.1: Predicted frequencies for *g*-EtSH from 8.7-26.5 GHz. The most intense peaks are seen from 18-26 GHz.

Most microwave components are frequency-dependent, so only a few components from the 8.7-18.3 GHz circuits are functional in the 18-26.5 GHz range. For this reason, a new circuit was built to extend the bandwidth from 18-26.5 GHz.

Waveform generation is essentially the same in both the 8.7-18.3 GHz and the 18-26.5 GHz circuits. The arbitrary function generator, AFG (Tektronix model AFG3252), arbitrary waveform generator, ARB (Tektronix model AFG7101), and phase-locked dielectric resonator oscillators (PLDRO) are each locked to a 10 MHz rubidium frequency standard (Stanford Research Systems FS725). The AFG generates a 2.5 ns, 2.5 volt square pulse that triggers the ARB to generate the

chirped pulse, which is 0.1 to 4.9 GHz for the 8-18 GHz bands or 0.35 to 4.6 GHz pulse for the 18-26 GHz band. In each band, the chirped pulse is filtered by a 5 GHz low pass filter, LPF (Lorch part number 8LA-5000-S) after the AWG. The pulse generator (Quantum Composer 9618, QC) and the oscilloscope are also triggered relative to the pulse. The QC controls the timing of the solid state amplifier (SSA) and the switch.

The signal from the PLDRO is split with a power divider. One leg is used as a local oscillator to upconvert the chirped pulse from the ARB with a double-balanced mixer (Miteq DM05020LW1). After the mixer, the upconverted chirped pulse passes through a pre-amp (Phase One Microwave SL-182010). The other leg is used to downconvert the chirped pulse before it enters the oscilloscope.

It is after the pre-amp that the 8.7-18.3 GHz and 18-26.5 GHz circuits begin to deviate. The lower band circuit (Fig. 3.2) uses the 13.6 GHz PLDRO filtered by a 13.6 ± 0.05 GHz band pass filter (BPF) (Lorch 4CF7-13600/100-S) and an 11.1 ± 2.4 GHz BPF (Lorch 13-IZ7-11100/4800-S) after the preamp. The middle band circuit uses the 18.4 GHz PLDRO filtered by an 18.4 ± 0.05 GHz band pass filter (BPF) (Lorch 4CF7-18400/100-S). This setup does not need a BPF before the preamp because the components do not transmit microwaves above 18 GHz.

In both the lower and middle bands, the pulse is then further amplified by a 10 W solid state amplifier (SSA) (Microwave Power L0619-40-T526), which is also controlled by the QC to be synced to the AWG so that it is only active when the

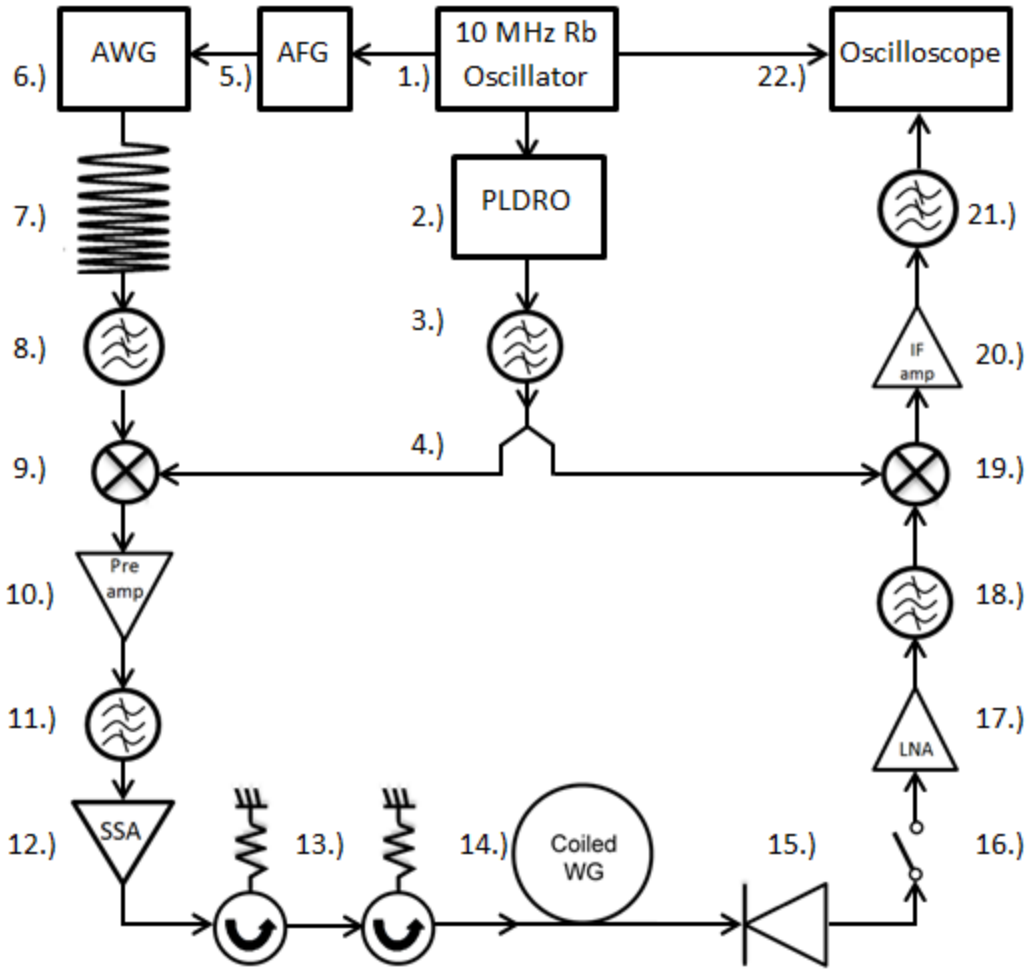

Figure 3.2: Circuit diagrams for the 8.7-18.3 GHz circuit

1.) 10 MHz rubidium frequency standard
2.) Phase-locked dielectric resonator oscillators (PLDRO). 13.6 GHz in lower band, 18.4 GHz in the middle band.
3.) Band Pass filter (BPF). 13.6 ± 0.05 GHz in the lower band 18.4 ± 0.05 GHz in the middle band.
4.) Wilkinson power divider
5.) The arbitrary function generator (AFG)
6.) arbitrary waveform generator (ARB)
7.) 250 ns chirped pulse from 0.1 to 4.9 GHz
8.) 5 GHz low pass filter (LPF)
9.) Mixer, upconverts the chirped pulse with the signal from the PLDRO
10.) Pre-amp
11.) 11.1 ± 2.4 GHz BPF, only in the lower band
12.) Solid state amp (SSA)
13.) Isolators
14.) Coiled waveguide
15.) Diode limiter
16.) Microwave switch
17.) Low noise amp (LNA)
18.) BPF. 11.1 ± 2.4 GHz in lower band, 15.9 ± 2.4 GHz in middle band
19.) Mixer, downconverts the chirped pulse with the signal from the PLDRO
20.) IF Amp
21.) 5 GHz LPF
22.) Oscilloscope

chirped pulse is present. Before entering the waveguide, the amplified pulse passes through single junction isolators (Ditom Microwave D317028). These prevent the pulse from reflecting back out of the waveguide and into the amplifier.

A low noise amplifier, LNA (Miteq AMF-5F-08001800-14-10P), is used in the receiver circuit to boost the molecular signal to detectable levels with minimal increase to the noise. Any components after the waveguide but before the LNA will lower the ultimate signal-to-noise ratio. Despite this, protection elements are still necessary to prevent user error from damaging the receiver. Therefore, the receiver circuit contains a diode limiter, DL (ACLM 4537-C361K) and switch (Advanced Technical Materials model S1517D). The DL limits the power of the pulse coming out of the waveguide so that it does not damage the LNA.

The amplified FID exiting the LNA is filtered by a BPF, 11.1 ± 2.4 GHz (Lorch 13-IZ7-11100/4800-S) in the lower band and 15.9 ± 2.4 GHz (Lorch 13-IZ7-15900/4800-S) in the middle band. The pulse then enters a second double-balanced mixer and is down converted with the other leg from the PLDRO (Fig. 3.2). The signal is further increased by an IF amplifier (B&Z Technologies, BZP106A) and filtered by a 5 GHz LPF (Lorch part number 8LA-5000-S) before being digitized by the oscilloscope (Tektronix TDS6154C). Besides the PLDROs and BPFs, the 8.7-13.5 GHz and 13.5-18.3 GHz circuits are identical, and as such are considered to be a single 8.7-18.3 GHz circuit.

The 18-26.5 circuit is the same as the lower band until item # 11 on Figure 3.2, but it then diverges (Fig. 3.3). After the pre-amp and BPF is an active frequency

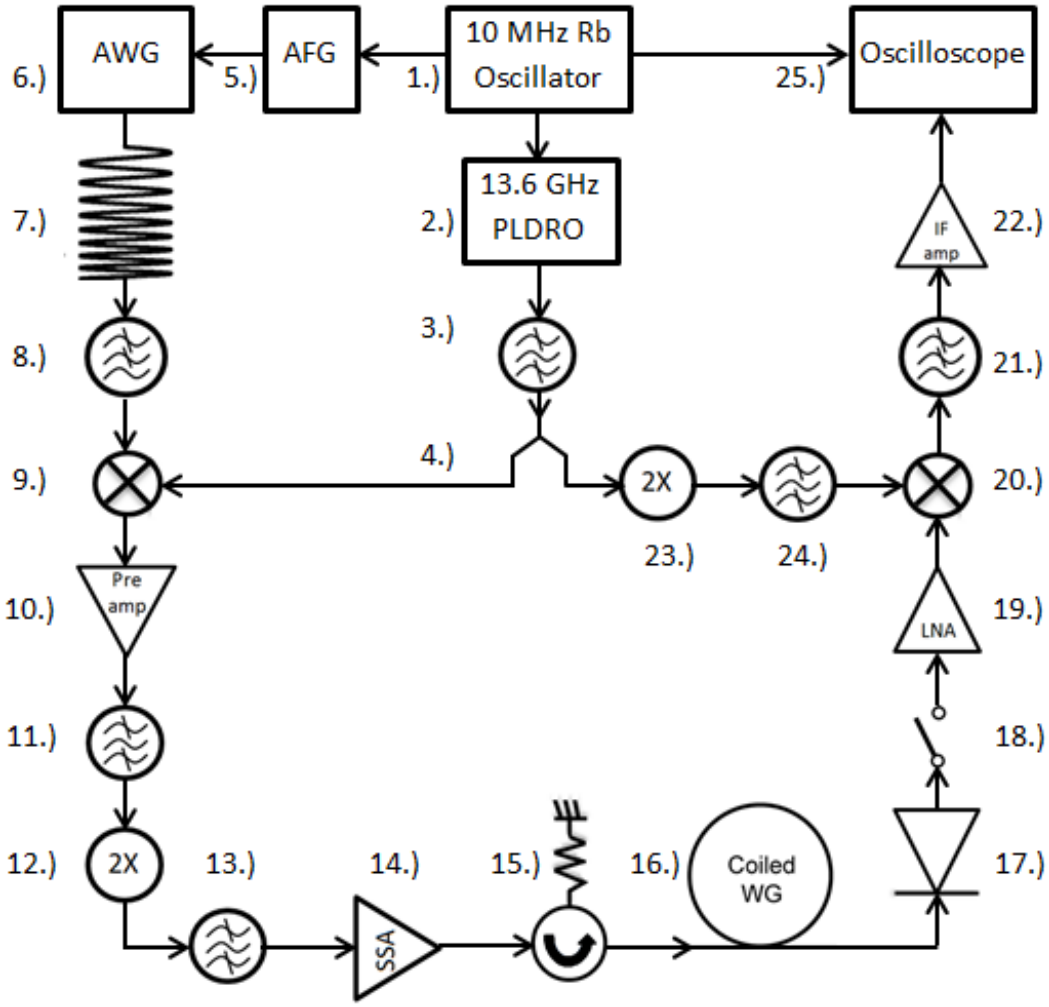

Figure 3.3: Circuit diagrams for the 18-26.5 GHz circuit

1.) 10 MHz rubidium frequency standard
2.) 13.6 GHz Phase-locked dielectric resonator oscillator (PLDRO)
3.) 13.6 ± 0.05 GHz Band Pass filter, BPF
4.) Wilkinson power divider
5.) The arbitrary function generator, AFG
6.) arbitrary waveform generator, ARB
7.) 250 ns chirped pulse from 0.35 to 4.6 GHz
8.) 5 GHz low pass filter, LPF
9.) Mixer, upconverts the chirped pulse with the signal from the PLDRO
10.) Pre-amp
11.) 11.1 ± 2.4 GHz BPF
12.) Frequency Doubler
13.) 22.25 ± 4.25 GHz BPF
14.) Solid state amplifier (SSA)
15.) Isolator
16.) Coiled waveguide
17.) Diode limiter
18.) Microwave switch
19.) Low noise amp (LNA)
20.) Mixer, downconverts the chirped pulse with the signal from the PLDRO
21.) 9.5 GHz LPF
22.) IF Amp
23.) Frequency doubler
24.) 27.200 ± 0.150 BPF
25.) Oscilloscope

doubler (Wright Technologies ATX26-220), which doubles the pulse frequency range to cover 18.0 to 26.5 GHz. The chirped pulse is then filtered by a 22.25 ± 4.25 GHz BPF (Lorch 131Z7-22250/8500-S), followed by 19 dB of attenuators before it enters the 4 W solid state amplifier (Microwave Power L1826-36T762). An 18-26.5 GHz isolator (Ditom Microwave D3I1826) is placed before the waveguide to protect the SSA from reflected high-powered microwaves. The sample cell is the same waveguide as in the 8.7-18.3 GHz circuit. After the waveguide, a diode limiter, DL (Advanced Control Components, ACLM-4765-C371K) and switch (MCLI D1-18/REF) precede the LNA (Miteq AMF- 6F-18002650-20-10P). Again, the DL and switch protect the LNA and the QC triggers when the switch opens or closes.

Unlike the 8-18 GHz circuit, a BPF does not precede the second mixer, which is a triple-balanced mixer (Miteq TB0440LW1) compatible with the 18-40 GHz region. Like the 8-18 GHz circuit, the second leg of the signal from the PLDRO is used to downconvert the pulse coming out of the waveguide. However, before the PLDRO output enters the second mixer, a frequency doubler (Wright Technologies ATX40-220) doubles the frequency to 27.2 GHz, after which it is filtered by a 27.200 ± 0.075 GHz BPF (Lorch 4CF7-27200/150-K). The down converted signal leaving the RF port of the triple-balanced mixer is between 0.7 and 9.2 GHz and filtered by a 9.5 GHz low pass filter (LPF) (Lorch 11LA-9500-S). The signal is then amplified by an IF amplifier (B&Z Technologies BZP110UB1X2) before entering the oscilloscope (Tektronix TDS6154C).

One problem with current data collection is that the waveguide is not designed to transmit light from 18-26 GHz. The WRD-750 waveguide used in the

spectrometer is optimized to guide microwaves between 8 and 18 GHz. Operating the waveguide at out-of-band frequencies drastically reduces the intensity of signal at certain frequencies in the 18-26 GHz region, which can be seen in Figure 3.4.

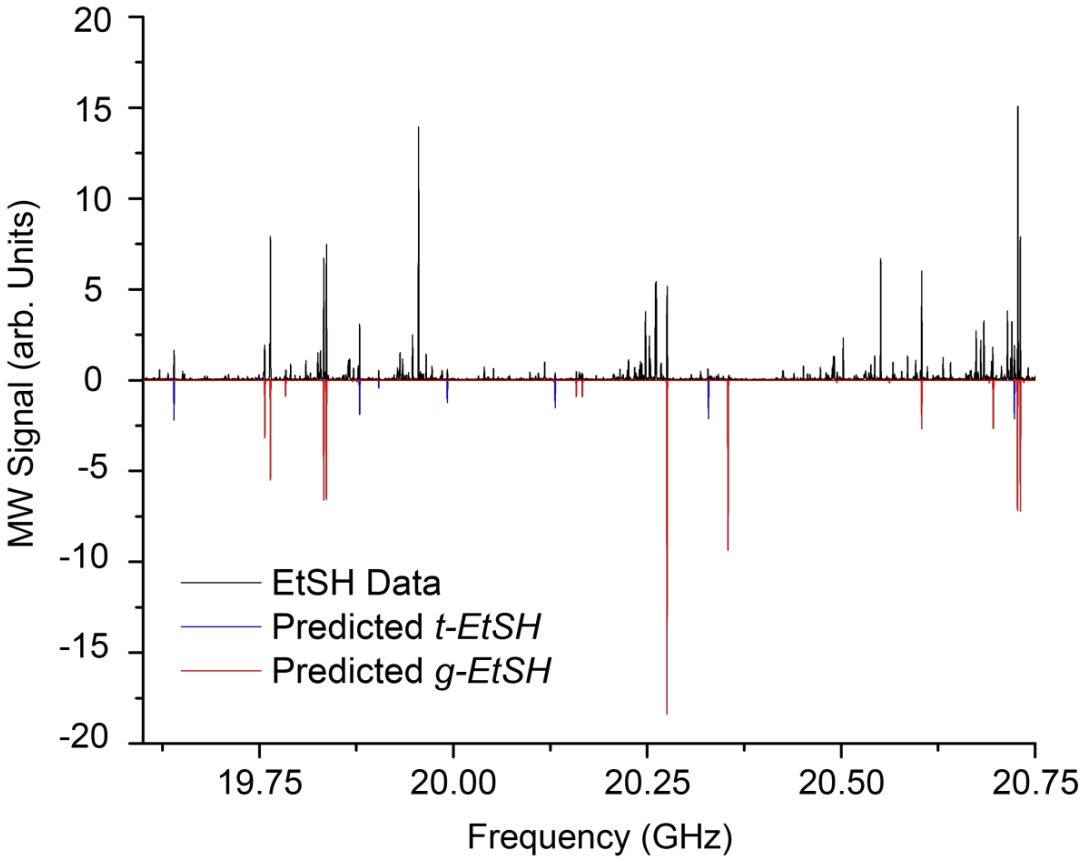

Figure 3.4: Poor relative intensities in the 18-26.5 GHz EtSH spectrum from operating the waveguide at out-of-band frequencies. The predicted intensity is significantly higher than the observed spectrum between 20.25 GHz and 20.5 GHz

Another complication of the 18-26 GHz band is that data collection is twice as slow because the sampling rate needs to be increased to 20 GS/s. After the chirped-pulse for the 18-26.5 GHz band is down converted, the signal at the oscilliscope is 8.5 GHz broad.

This means that the sampling rate must be increased to at least 17 GS/s. The closest setting to this on the oscilliscope is 20 GS/s, and so twice as many samples are collected per average compared to the 8-18 GHz setup. This requirement is due to the Nyquist-Shannon sampling theorem, which says that the sampling rate must be at least twice that of the maximum frequency in order to completely determine the signal.

Another improvement that has been made to the spectrometer is the construction of a flow-through waveguide chiller. At higher temperatures, more states are populated, which manifests in the spectrum as more peaks. This increases the difficulty of fitting not only due to the larger number of peaks but also because the rotational energy is more dispersed and so the intensities of all transitions decrease, making the signal harder to distinguish from the noise.

For this reason, we designed a cooling system that can lower the waveguide temperature to -25 °C. The details of the cooling system are described in Maria Phillips' senior thesis. [10]

4: Ethanethiol

Ethanethiol, EtSH, (Fig. 4.1) was chosen for study for several reasons. It is a small slightly asymmetric prolate top with a high vapor pressure and a strong dipole moment. As previously discussed, it is also a molecule of interest for astrochemistry. EtSH has two stable conformers, the *trans* and the *gauche,* with 1.58 ± 0.04 D and 1.61 ± 0.05 D dipole moments, [11] respectively. *Ab initio* calculations showed that the *gauche* conformer is more stable than the *trans* conformer by 213.3 cm^{-1}, and so it is more abundant. The *gauche* spectrum is complicated because the thiol H-atom can be offset from the symmetry plane in either direction, producing two conformers that are mirror images of one another, referred to as *gauche* and *gauche'*. The conformers are degenerate, but tunneling interactions break their symmetry. This leads to significant splitting that can be observed in the spectrum.

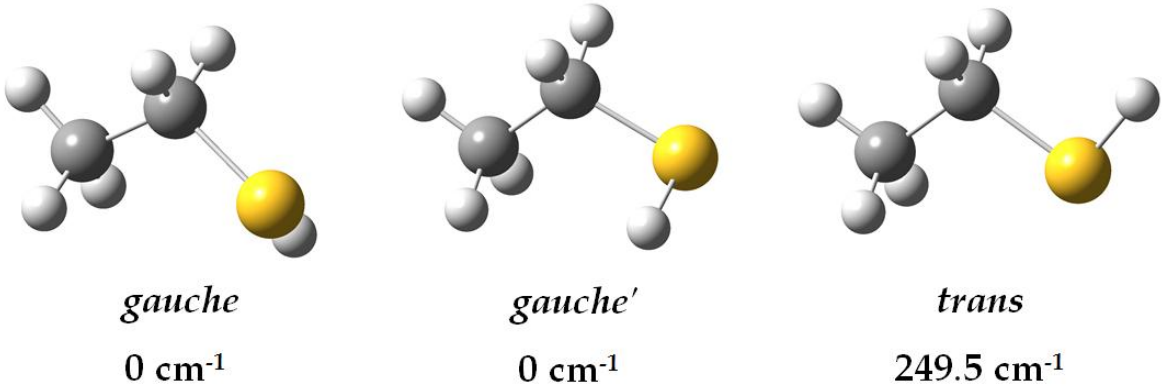

Figure 4.1: The stable conformers of EtSH

Tunneling of the thiol H allows *g*-EtSH and *g'*-EtSH to interconvert (Figure 4.2). The tunneling process breaks the degeneracy between the two mirror forms, producing symmetric (+) and antisymmetric (-) torsional substates of the *gauche*

conformer. This can be seen as tunneling splittings in the observed spectrum that are as large as 3.5 GHz. [12]

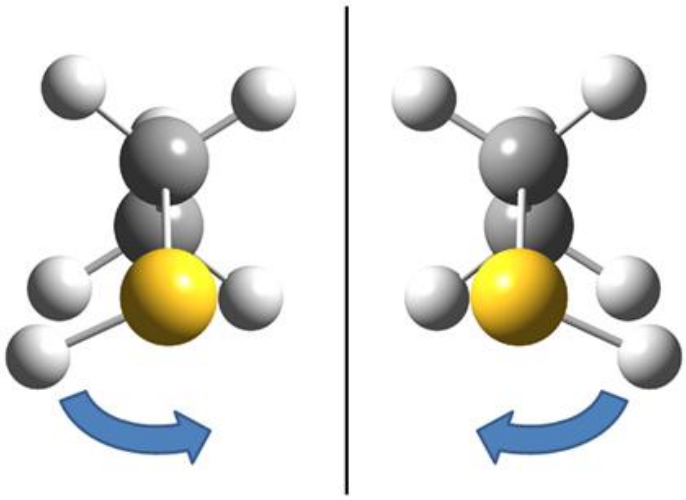

Figure 4.2: The thiol H-atom tunneling through the potential barrier

The *c*-dipole transitions are split above and below their rigid rotor predictions by the tunneling frequency, which is the frequency with which the thiol H-atom tunnels between its two equivalent *gauche* configurations. [12] These splittings cannot be predicted using a rigid rotor model. To fit the spectra, a more complete Hamiltonian needs to be used which incorporates symmetric and antisymmetric constants and cross terms that allow for transitions between the two substates.

The *trans* conformer does not exhibit the tunneling splitting seen in the *gauche* conformer and can be fit using a standard Watson A-reduced Hamiltonian. It has no *c*-dipole moment because the thiol H-atom is in the symmetry plane. *Ab initio* calculations indicate that the barrier to internal rotation for the methyl rotor is sufficiently high that transitions are predicted to be observed as singlets at our resolution. However, since it is less abundant, the intensities of its transitions are

lower than those of the *gauche* conformer. This hinders the fitting process because many transitions can be obscured by larger *gauche* peaks or lost in the noise.

The rotational spectrum of ethanethiol has been studied extensively by several groups. It was first studied by Imanov *et al.* in 1967 from 18-33 GHz at 228 K using a Stark-modulated spectrometer. [13] In 1968, Kadzhar *et al.* studied its spectrum at 223 K with a Stark-modulated spectrometer, also from 18-33 GHz. [14] The ^{34}S and ^{13}C species were also measured at 194.5 K.

In 1974, Hayashi *et al.* published a paper focusing on the *trans* conformer at dry ice temperature using a Stark-modulated spectrometer in frequency region 8.4-34 GHz. They observed peaks from the *trans* conformer as singlets and assigned 21 lines up to J = 7 from both *a*- and *b*-type transitions in the ground vibrational state. Some progress was also made towards fitting the ^{34}S and ^{13}C species but most *a*-type transitions were obscured by strong transitions from the normal species.

Schmidt *et al.* published a comprehensive paper on both the *trans* and the *gauche* conformers in 1975 at room temperature from 12.0 to 40.0 GHz on a Stark-modulated spectrometer [15]. They used second-order Stark effects to determine the a-, *b*-, and *c*-dipole moments for each conformer, which are reported in Table 4.1.

Table 4.1: Dipole Moments for EtSH			
	*Ab Initio**	Schmidt [11]	Nakagawa [12]
g-EtSH			
μ_a (D)	1.61	1.49 (2)	-
μ_b (D)	0.15	0.19 (10)	-
μ_c (D)	0.72	0.59 (2)	-
μ_{total} (D)	1.78	1.61 (5)	-
t-EtSH			
	*Ab Initio**	Hayashi[15]	Schmidt [11]
μ_a (D)	1.055	1.06(3)	1.058(3)
μ_b (D)	1.49	1.17(3)	1.146(2)
μ_c (D)	0.0022	0	0
μ_{total} (D)	1.830	1.58(4)	1.560(32)

* Calculated at the B3LYP/6-311++G(d,p) level of theory in Gaussian 09.

For the *trans* conformer, Schmidt *et al.* assigned 46 lines to J = 18. [11] All of the identified lines were *b*-type transitions except for ^aR lines with J ≤ 4. They were able to observe fine structure with small splittings of about 100 kHz at higher J which they attributed to the effects of internal rotation of the methyl group.

They determined that the barrier to internal rotation of the methyl group of the *trans* conformer was V_3=1156 ± 30 cm^{-1}. Additionally, 17 lines up to J=9 were assigned to the v = 1 thiol torsion vibrational state, which was approximately half the intensity of the *trans* normal species.

Schmidt *et al*. also made significant progress in fitting the more challenging *gauche* conformer. Selection rules describe the allowed transitions between the symmetric and antisymmetric states. The selection rules for the *gauche* conformer are that *a*-type transitions are allowed between two symmetric states or two antisymmetric states (+ ↔ + and – ↔ –) while *c*-type transitions are only allowed between a symmetric state and an antisymmetric state (+ ↔ –).

Using these selection rules, they created a more complete Hamiltonian that included terms for the symmetric and antisymmetric states, as well as cross terms for transitions connecting these states. Their Hamiltonian is shown below and the resulting energy level diagram is in Figure 4.3. The terms in this Hamiltonian are explained in Table 4.2.

$$\hat{H}_{++} = A_+ \hat{J}_a^2 + B_+\hat{J}_b^2 + C_+\hat{J}_c^2 \quad (4.1)$$

$$\hat{H}_{--} = A_-\hat{J}_a^2 + B_-\hat{J}_b^2 + C_-\hat{J}_c^2 + \Delta\nu \quad (4.2)$$

$$\hat{H}_{+-} = D_\pm (\hat{J}_c\hat{J}_b + \hat{J}_b\hat{J}_c) + E_\pm (\hat{J}_b\hat{J}_a + \hat{J}_a\hat{J}_b) + N_\pm\hat{J}_b + Q_\pm\hat{J}_a \quad (4.3)$$

Table 4.2: Terms of *g*-EtSH Hamiltonian from Schmidt *et al.* [11]

Symmetric state (+) rotational constants	Antisymmetric state (-) rotational constants	Cross Terms connecting the (+) and (-) states	Energy separation of (+) and (-) states	Operators
A_+	A_-	$D_\pm$		$(\hat{J}_c\hat{J}_b + \hat{J}_b\hat{J}_c)$
B_+	B_-	$E_\pm$	$\Delta\nu$	$(\hat{J}_b\hat{J}_a + \hat{J}_a\hat{J}_b)$
C_+	C_-	$N_\pm$		$\hat{J}_a^2$, $\hat{J}_b^2$, and $\hat{J}_c^2$
		$Q_\pm$		

For the *gauche* conformer, Schmidt *et al.* observed strong *a*-type transitions as doublets with splittings of up to 9 MHz as well as *c*-type transitions that were split by ~3.5 GHz. The energy separation between the symmetric and antisymmetric state, Δν, is the primary contribution to the splitting in *g*-EtSH. Therefore, the tunneling frequency can be approximated to be equal to Δν, which they found to be 1754 MHz for the ground state normal species. [11] They did not include any of the cross term coefficients in their fit. The $D_\pm$ and $E_\pm$ parameters were approximated, but they had a high uncertainty and were not included in the fit.

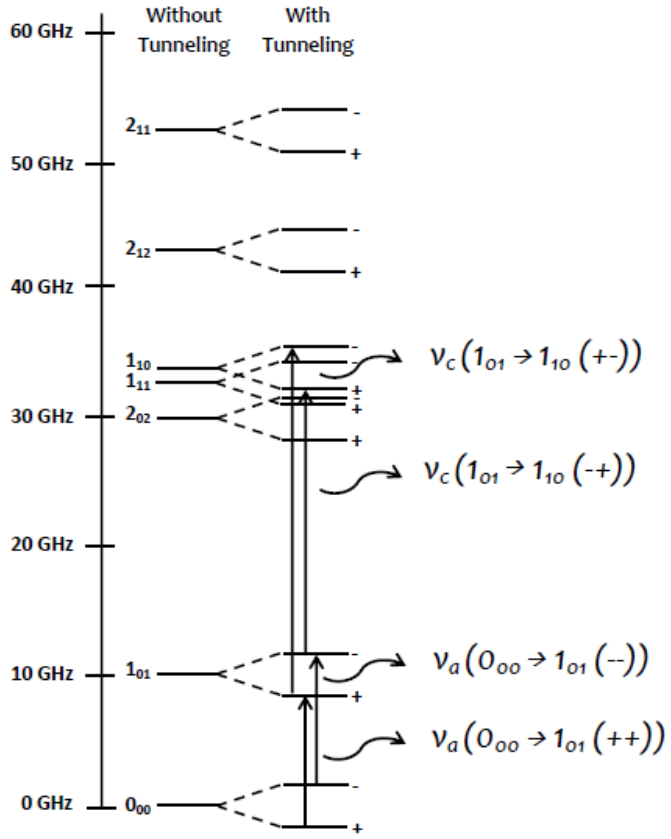

Figure 4.3: Energy level diagram of *gauche* EtSH, adapted from Schmidt and Quade[11]

Schmidt *et al.* also assigned 10 *a*-type transitions to J=3 in the v=1 thiol torsion excited state. However, no *c*-type transitions could be assigned, partially due to their low intensity but mostly due to their substantial predicted splitting of 3.5 GHz. Since only *a*-type transitions were assigned, the A rotational constant could not be well determined. However, the authors provided estimates of 5292.17 MHz and 4839.82 MHz for the B and C rotational constants, respectively, based on the center frequencies of the observed doublets.

In 1976, Nakagawa *et al.* published a continuation of their previous work on EtSH[15] focusing on the *gauche* conformer using the same instrumentation and conditions as before.[15],[12] Their findings closely matched the work of Schmidt *et al.*

and they analyzed their data with the same Hamiltonian. They did include one cross term, $D_{\pm}$, that they allowed to vary in their fit and found to be 12.43 (37) MHz. They fit 31 lines to J=4 of the ground state normal species of EtSH. Additionally, they assigned 21 lines up to J= 4 to the ^{34}S and both ^{13}C isotopomers.

Even though this molecule has been extensively studied, our chirped-pulse spectrometer is much more sensitive than previous Stark-modulated instruments. Additionally, several sophisticated fitting programs have been developed in the last four decades which dramatically improve the fitting process.

Before beginning considering the spectrum, several *ab initio* calculations were performed on both conformers at the B3LYP/6-311G++(d,p) level of theory in Gaussian 09. Geometric optimizations showed that the *gauche* conformer was the lower energy state by 213.3 cm^{-1}. The thiol H-atom was calculated to be in the plane of symmetry at 180° for the *trans* conformer and is offset from the symmetry plane by 62.47° or -62.47° for the *gauche* and *gauche'* conformers, respectively.

Separate 1D potential energy scans were performed on the optimized structures for the methyl rotor dihedral and the thiol rotor dihedral. Each calculation scanned the potential energy over 360° about the dihedral angle in a series of 36 steps of 10°. The thiol dihedral scan (Fig. 4.4) was fit to a $V_2 + V_3$ potential the methyl dihedral scans (Fig.4.5) were fit to a V_3 potential. The results of those scans are listed in Table 4.3.

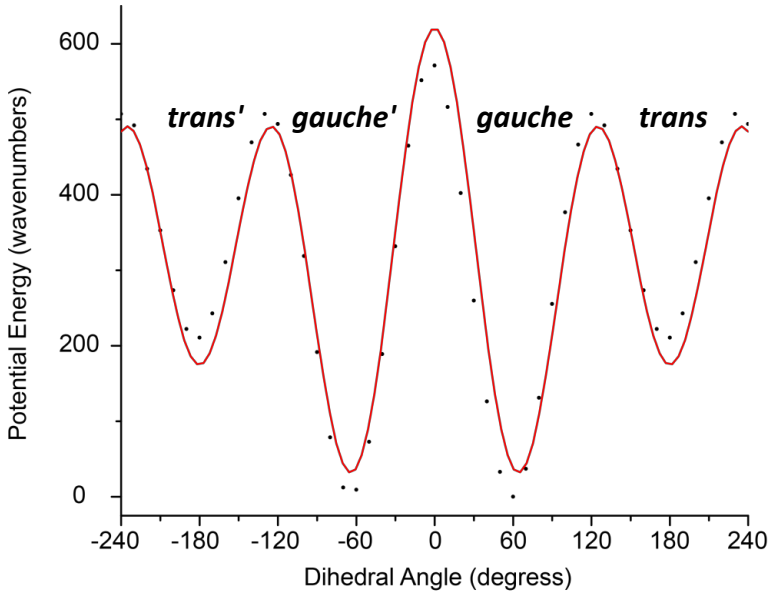

Figure 4.4: Thiol torsion dihedral 1D potential energy scan of EtSH at the B3LYP/6-311G++(d,p) level of theory in Gaussian 09. Black circles are the calculated points and the red line is the V_3 potential energy fit.

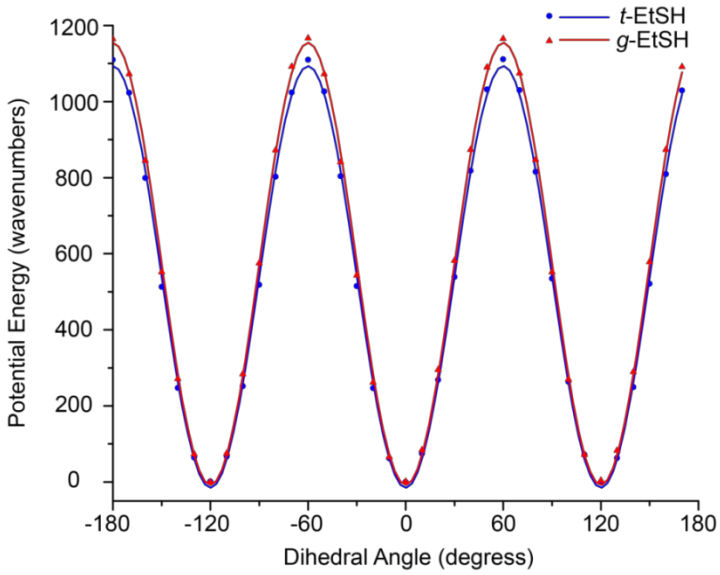

Figure 4.5: Methyl torsion dihedral 1D potential energy scan of *t*-EtSH and *g*-EtSH at the B3LYP/6-311++G(d,p) level of theory in Gaussian 09. For both, the symbols are the calculated points and the line is the V_3 potential energy fit.

Table 4.3: Barrier Potentials for EtSH				
	Schmidt [11]	Nakagawa[12]	*Ab Initio*	
Thiol Torsion Fits (cm^{-1})				
V_1	-65	-72.4 (67)	0 (fixed)	
V_2	-135	-135 (27)	-152.28 (18)	
V_3	440	456.4 (20)	451.68 (17)	
Methyl Torsion Fits (cm^{-1})				
	Schmidt [11]	Nakagawa[12]	*Ab Initio**	
			gauche	*trans*
V_3	1156 (30)	1140.2 (30)	1162.72 (7)	1109.04 (6.3)

*Calculated at the B3LYP/6-311++G(d,p) level of theory in Gaussian 09.

In both the *trans* and the *gauche* conformers, the barrier of the methyl rotor is sufficiently high to hinder internal rotation. Thus, any splitting in the transitions of the *trans* conformer is expected to be too small to resolve on our instrument.

Anharmonic frequency calculations were performed in the center of mass frame of reference. This provides the anharmonically corrected vibrational frequencies and vibration-rotation coupling constants for the vibrational excited states, the first five of which are listed in Table 4.4. Since the *gauche* conformer is the lower energy state, all energies are scaled using *g*-EtSH ground state as a zero, though it is important to note that it is not zero point corrected. The abundances of the other species have also been calculated relative to *g*-EtSH. (Table 4.4)

It can be seen that the *trans* conformer is only expected to be 15% of the intensity of the *gauche* conformer. Furthermore, the first three *gauche* vibrational states are predicted to be more intense or equal to the trans conformer. This significantly increases the difficulty of fitting the *trans* spectrum because it becomes very difficult to differentiate between gauche excited state transitions and ground state *t*-EtSH transitions.

This output also provides the dipole moments as well as the rotational and distortion constants for each conformer. The *ab initio* dipole moments were previously given in Table 4.1, as well as the previous values from the literature. The rotational and distortion constants are in Tables 4.5 and 4.6 for the *gauche* and *trans* conformers, respectively.

Table 4.4: Calculated anharmonic vibrational energies, relative intensities and vibration-rotation coupling constants for EtSH [a]

Description	ΔE (cm^{-1})[b]	Pred. Int. (250 K)[c]	α_A (MHz)	A_B (MHz)	A_C (MHz)
g-EtSH					
Ground State	0	1	-	-	-
Thiol torsion	212.30	0.30	20.9030	0.70880	7.33213
Methyl torsion	260.60	0.233	93.42602	18.32746	9.44624
Backbone scissors	327.40	0.152	-292.4968	4.38466	9.42722
C-S stretch	645.79	0.024	-1.89535	28.19434	25.12237
Backbone twist	741.29	0.014	-56.95803	16.47259	12.69370
***t*-EtSH**					
Ground State	213.32	0.15	-	-	-
Thiol torsion	374.08	0.058	21.82703	33.46728	7.63495
Methyl torsion	466.27	0.034	207.17790	13.22978	7.33624
Backbone scissors	515.31	0.026	-354.9053	-0.95101	7.66273
C-S stretch	869.76	0.003	3.62855	30.69797	27.51731
Backbone twist	1005.64	0.002	-4.76068	11.62946	11.40539

a) Calculated at the B3LYP/6-311++G(d,p) level of theory in Gaussian 09.
b) Not zero-point corrected. Scaled using the ground state *g*-EtSH as a zero
c) Includes two-fold degeneracy of *gauche* conformer

The spectrum of ethanethiol was collected from 8.7 to 26.5 GHz at ~256 K and 6 mTorr. We collected 2 million averages across the full bandwidth, as well as a blank at high pressure that was subtracted from the data set. The collected spectrum is incredibly dense because of the large number of conformers and

vibrational states presents at ~256 K. The full spectrum can be seen in Figure 4.6 with the blank overlaid in red.

To fit the *gauche* conformer, we combined constants from the Hamiltonian used in the fit reported by Nakagawa *et al.*,[12] with the quartic distortion constants from the Watson A-reduced Hamiltonian to create a new Hamiltonian:

$$\hat{H} = \hat{H}_{++} + \hat{H}_{--} + \hat{H}_{+-} + \hat{H}_d^{\{4\}} \tag{4.5}$$

$$\hat{H}_{++} = A_+ \hat{J}_a^2 + B_+ \hat{J}_b^2 + C_+ \hat{J}_c^2 \tag{4.6}$$

$$\hat{H}_{--} = A_- \hat{J}_a^2 + B_- \hat{J}_b^2 + C_- \hat{J}_c^2 + \Delta\nu \tag{4.7}$$

$$\hat{H}_{+-} = D_{\pm} (\hat{J}_c \hat{J}_b + \hat{J}_b \hat{J}_c) \tag{4.8}$$

$$\hat{H}_d^{\{4\}} = -D_J \hat{J}^4 - D_{JK} \hat{J}^2 \hat{J}_c^2 - D_K \hat{J}_c^4 - 2d_J \hat{J}^2 (\hat{J}_a^2 - \hat{J}_b^2) - d_K [\hat{J}_c^2 (\hat{J}_a^2 - \hat{J}_b^2) + (\hat{J}_a^2 - \hat{J}_b^2) \hat{J}_c^2] \tag{4.9}$$

We began our analysis by using the rotational constants from Nakagawa *et al.* for the *gauche* conformer[12] and Hayashi *et al.* for the *trans* conformer[15]. In both cases, we used the distortion constants from *ab initio* calculations (Table 4.5 and 4.6). Out of 1912 lines above the 3:1 noise threshold, 129 were assigned. 44 lines up to J=15 were assigned to the ground state normal species of the *gauche* conformer and 85 lines up to J=36 were assigned to the ground state normal species of the *trans*. The results of these fits can be seen in Tables 4.5 and 4.6 for the *gauche* and *trans* conformers, respectively.

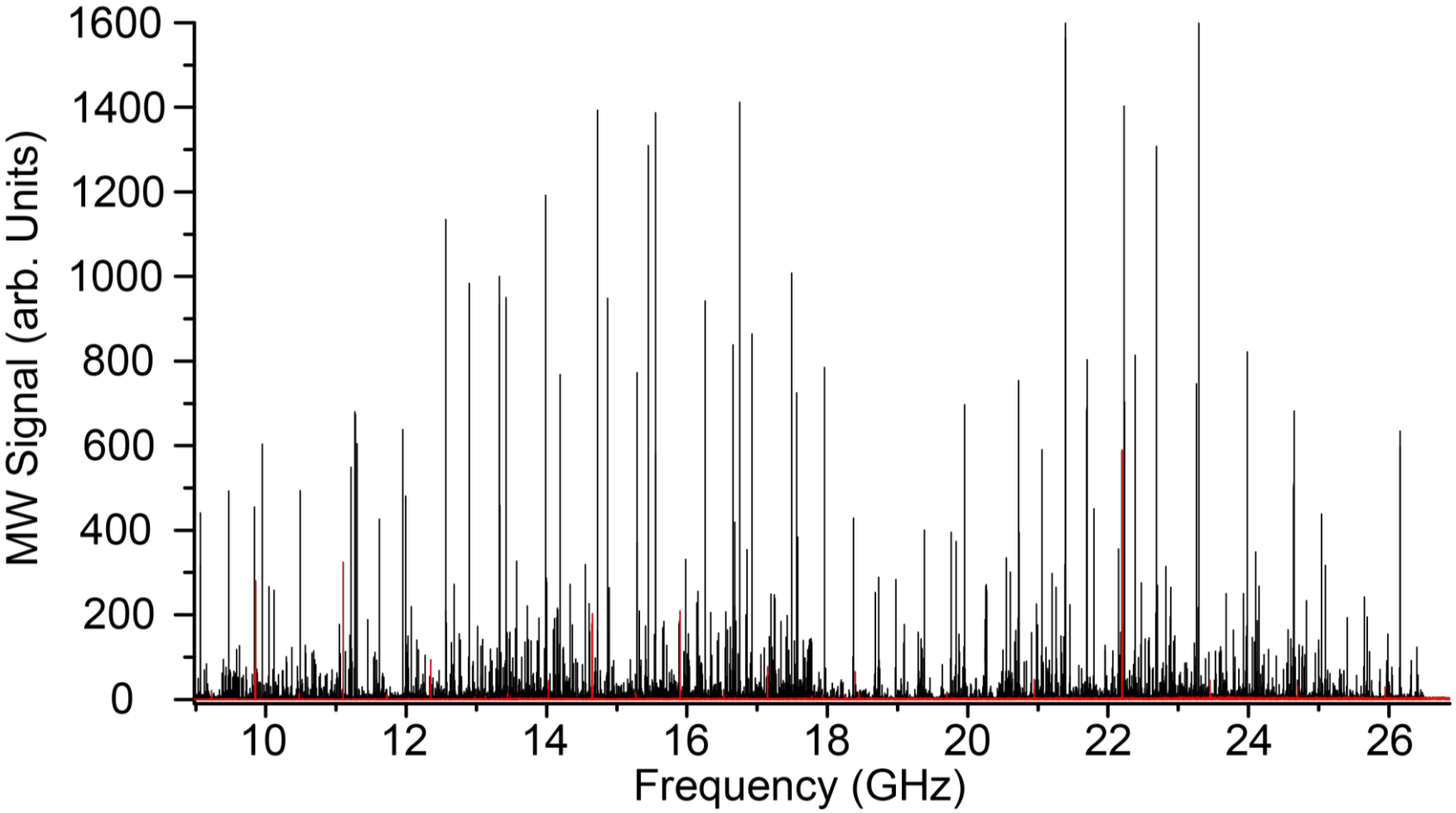

Figure 4.6: Full spectrum of EtSH from 8.7 to 26.5 GHz (black) at 256 K, 6 mTorr, and 2 million averages. The noise level (red) is at 5 intensity units. There are 1912 peaks above the 3:1 signal-to-noise cutoff.

Table 4.5: Rotational constants for the ground state normal species of *g*-EtSH				
Parameter	*Ab Initio* [a]	Schmidt [11]	Nakagawa [12]	Observed [b]
A (MHz)	28957.73	28746.37 (3)	28747.09 (50)	28749 (92)
B (MHz)	5173.57	5294.85 (3)	5294.78 (12)	5294.86 (12)
C (MHz)	4754.44	4846.96 (3)	4846.18 (12)	4846.11 (11)
Δv (MHz)	-	-	1753.84 (29)	1760 (76)
D± (MHz)	-	12.20	12.43 (37)	12.29 (107)
E± (MHz)	-	139.34	-	-
D_J (MHz)	0.0032	-	-	0.0032
D_{JK} (MHz)	-0.018	-	-	-0.018
D_K (MHz)	0.21	-	-	1.9 (167)
d_J (MHz)	0.47E-03	-	-	0.47E-03
d_K (MHz)	0.0087	-	-	0.0087
Lines Fit	-	40	26	44
Fit RMS (MHz)	-	0.03	-	0.042
Max J	-	8	4	15

a) Calculated at the B3LYP/6-311++G(d,p) level of theory in Gaussian 09.
b) If no uncertainty reported, parameter was locked to ab initio values.

Table 4.6: Rotational constants for the ground state normal species of *t*-EtSH				
	Ab Initio[a]	Hayashi [15]	Schmidt [11]	Observed [b]
A (MHz)	28676.75	28416.89(74)	28416.59(3)	28416.752(235)
B (MHz)	5352.87	5485.77(9)	5485.76(3)	5485.785(50)
C (MHz)	4780.86	4881.92(10)	4881.81(3)	4881.823(42
D_J (MHz)	0.0037	-	-	0.00388 (35)
D_{JK} (MHz)	-0.022	-	-	-0.0218(50)
D_K (MHz)	0.20	-	-	0.2065(94)
d_J (MHz)	0.00059	-	-	6.576(247)E-04
d_K (MHz)	0.0059	-	-	0.00734(218)
Lines Fit	-	21	46	85
Fit RMS (MHz)	-	0.22	0.03	0.077
Max J	-	7	18	36

a) Calculated at the B3LYP/6-311++G(d,p) level of theory in Gaussian 09. If no
b) uncertainty reported, parameter was locked to ab initio values.

The quality of the fit can be seen in Figure 4.7, which shows the agreement between the observed *gauche* transitions (black) against the predicted spectrum (red) generated by our experimental constants.

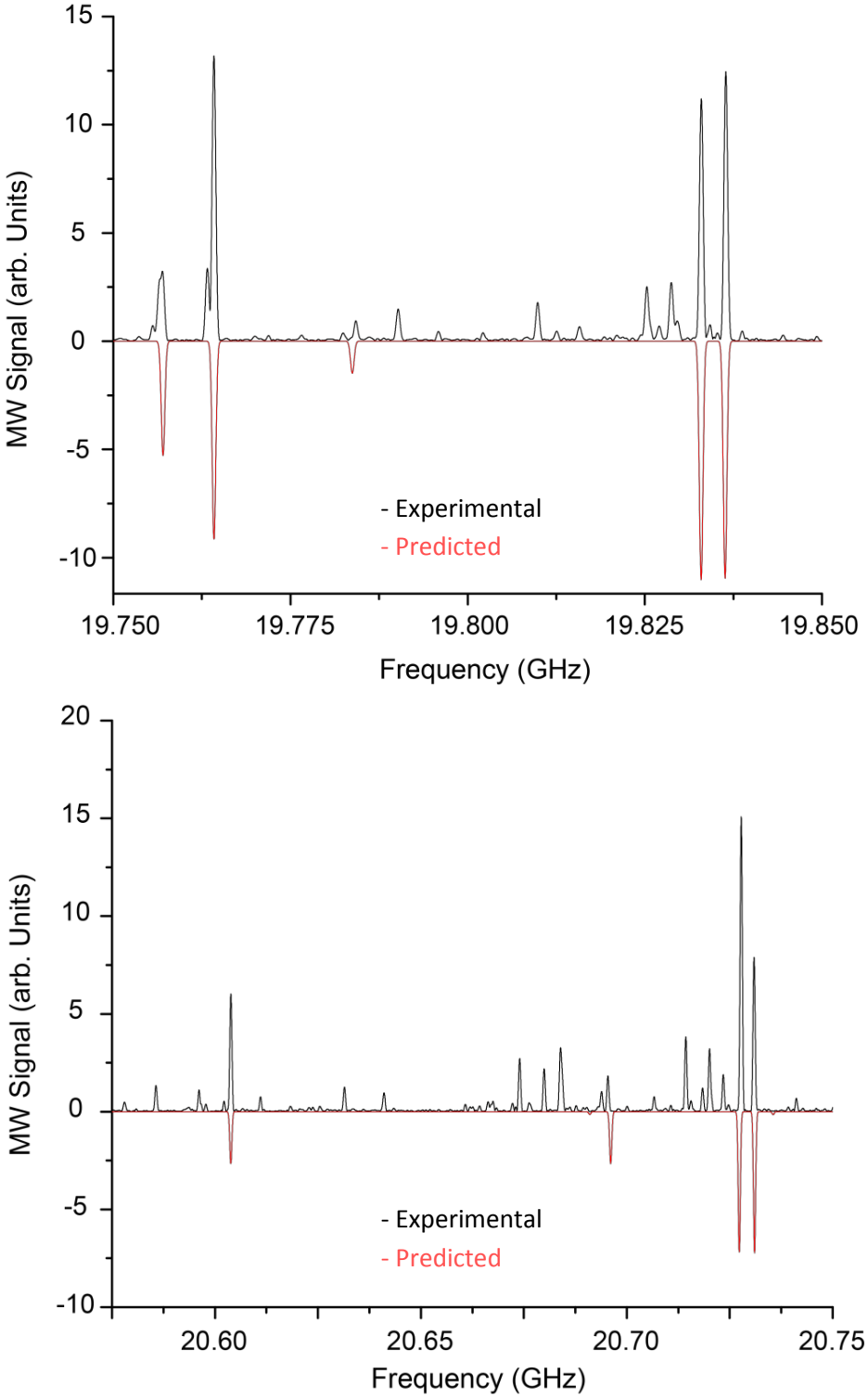

Figure 4.7: Expanded view of the experimental spectrum of EtSH from versus simulated data from the experimental *gauche* conformer rotational constants on the negative scale.

Once the correct Hamiltonian was in use, the *gauche* spectrum was able to be fit using SPFIT/SPCAT. Large tunneling splittings of ~3500 MHz were observed in the *c*-type transitions. The tunneling frequency, Δv, was fit to be 1760 ±76 MHz. The parameter D± from was included in the fit and its initial value was set to the previous result from Nakagawa, *et* al,[12] which was reported above in Table 4.5.

The *trans* conformer could be predicted using the Watson A-reduced Hamiltonian. As predicted, its spectrum was much less intense thsn the *gauche* conformer and many of the *t*-EtSH transitions were overlapped by stronger *g*-EtSH lines or in the noise. Despite this, 85 transitions up to J=36 were assigned to the *trans* conformer with a 0.077 MHz RMS. The rotational constants for this conformer are listed in Table 4.5.

The expanded view in Figure 4.8 shows that the predicted peaks are in good agreement with the experimental data, plotted in black, with the predicted *trans* spectrum (blue) which was generated from our experimental constants

In both Figure 4.7 and 4.8, it can be seen that out of almost 18 GHz of frequency bandwidth, our predicted peaks agree with our observed spectrum to within tens of kHz. The entire predicted *trans* (blue) and *gauche* (red) spectra have been simulated against the experimental data for each frequency range in Figures 4.9, 4.10, and 4.11.

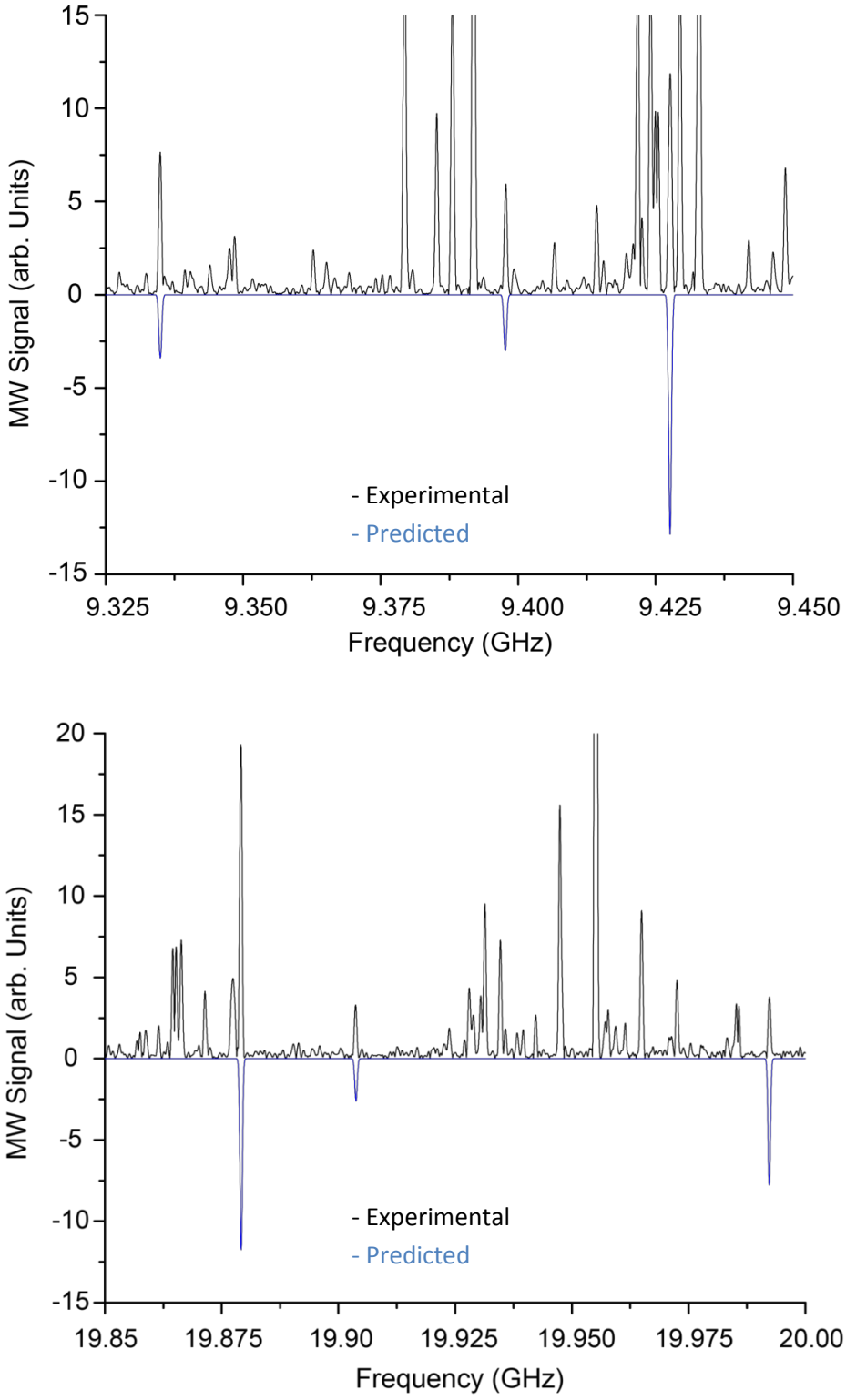

Figure 4.8: Expanded view of the experimental spectrum (black) of EtSH versus simulated data from the experimental *trans* conformer (blue) rotational constants on the negative scale.

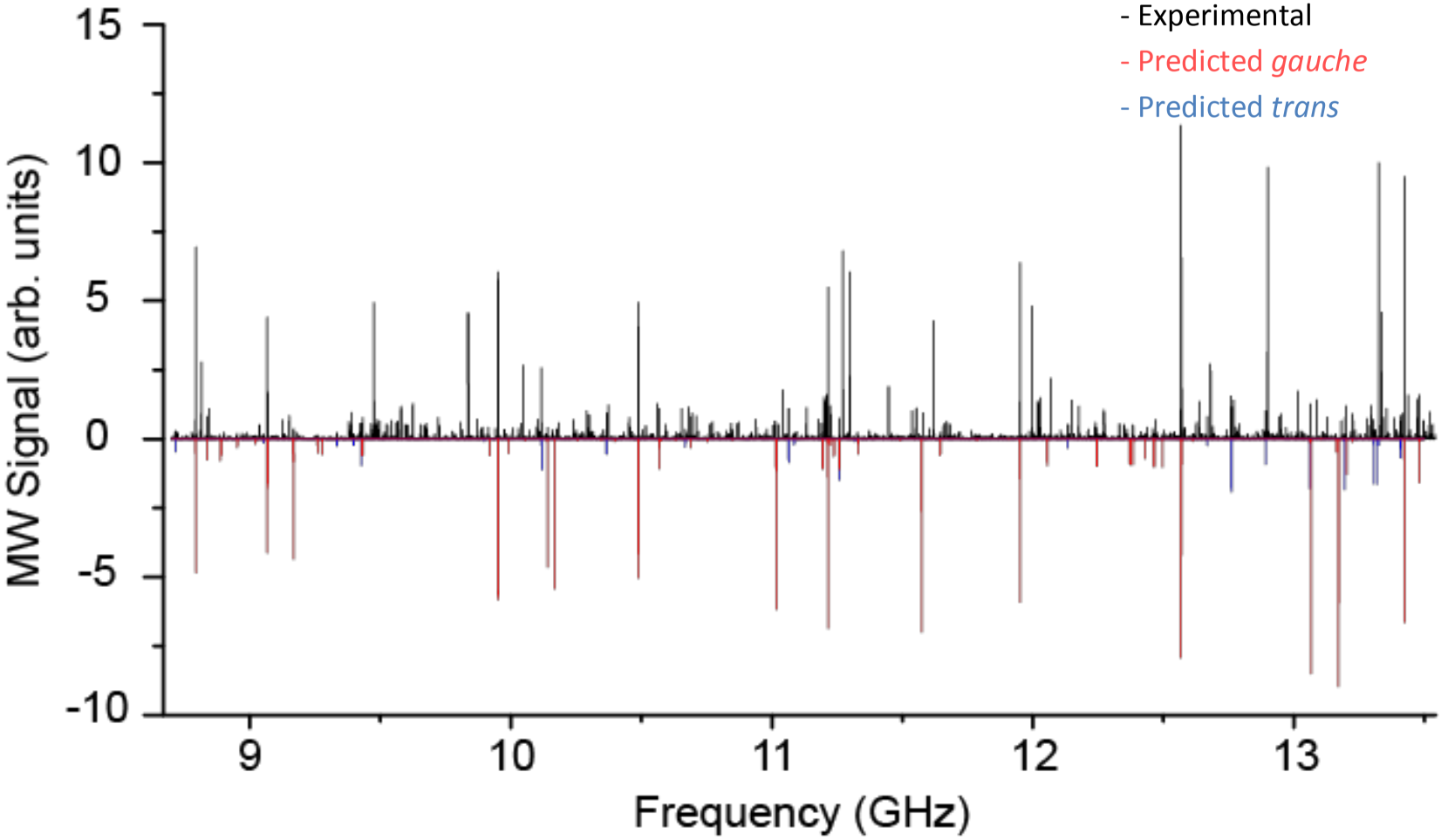

Figure 4.9: Experimental spectrum of EtSH from 8.7 to 13.5 GHz against simulated data from the experimental rotational constants on the negative scale. The predicted *gauche* is simulated in red and the predicted *trans* spectrum is simulated in blue.

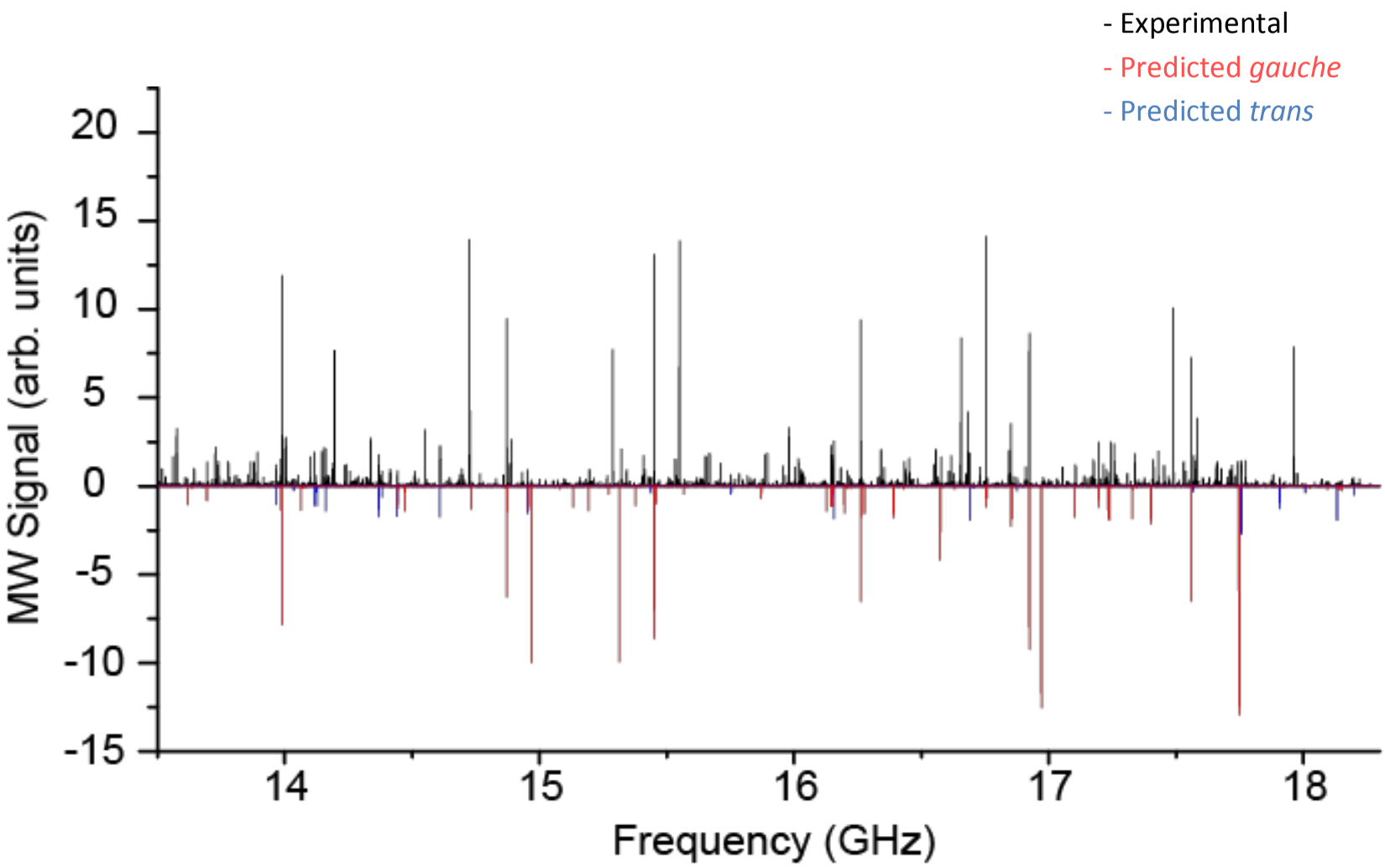

Figure 4.10: Experimental spectrum of EtSH from 13.5 to 18.3 GHz against simulated data from the experimental rotational constants on the negative scale. The predicted *gauche* is simulated in red and the predicted *trans* spectrum is simulated in blue.

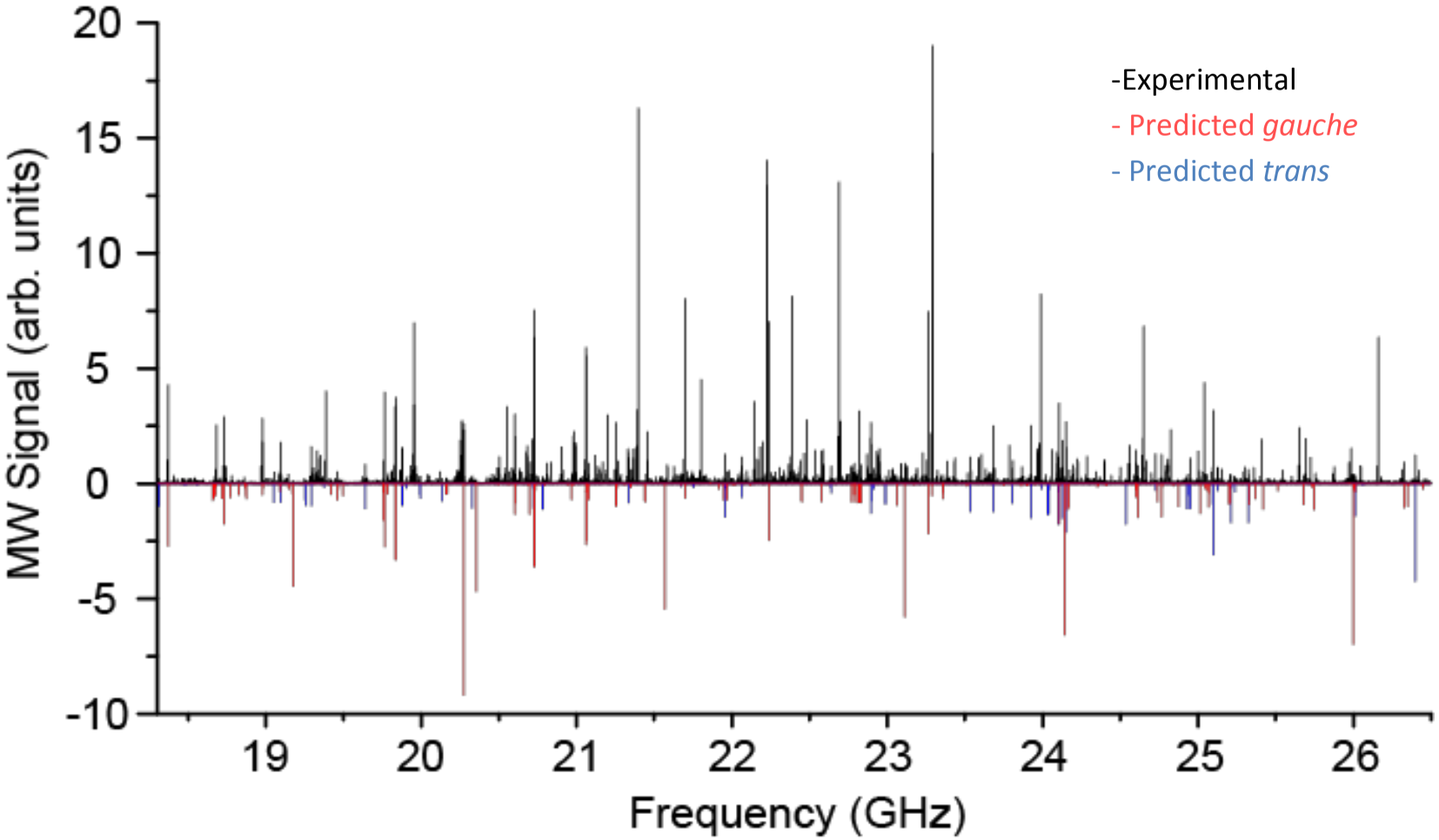

Figure 4.11: Experimental spectrum of EtSH from 18.3 to 26.5GHz against simulated data from the experimental rotational constants on the negative scale. The predicted *gauche* is simulated in red and the predicted *trans* is spectrum simulated in blue.

The observed spectrum is incredibly dense because of the large number of conformers and vibrational states present. We are able to observe some ground state *gauche* conformer ^{34}S transtions (Figure 4.12) but they are very close to the 3:1 signal to noise cutoff. Since data below the cutoff is unreliable, we are currently unable to fit this spectrum.

However, our lab will soon receive a new digitzer which will increase our rate of data collection by at least a factor of 60. This will allow us to collect many more averages in a very short period of time. Since our spectrometer's detection of the FID is phase sensitive, there is no apparent noise floor. The resolution of the observed spectra is limited by the length of the FID. With the new odigitizer we will be able to collect more averages and use a longer FID, so have less noise and a higher resolution. We should then be able to observe isotopomers and excited states that are currently lost to the noise.

Besides increasing our resolution, the next step towards fitting ethanethiol is to be able to fit higher J transitions. This is challenging in our current bandwidth because many of the strong high J transitions are above 26.5 GHz. Additional data outside of our current bandwidth is needed to move on to higher J values. This will soon be accomplished because a new spectrometer will be built this summer that will operate from 110 to 170 GHz.

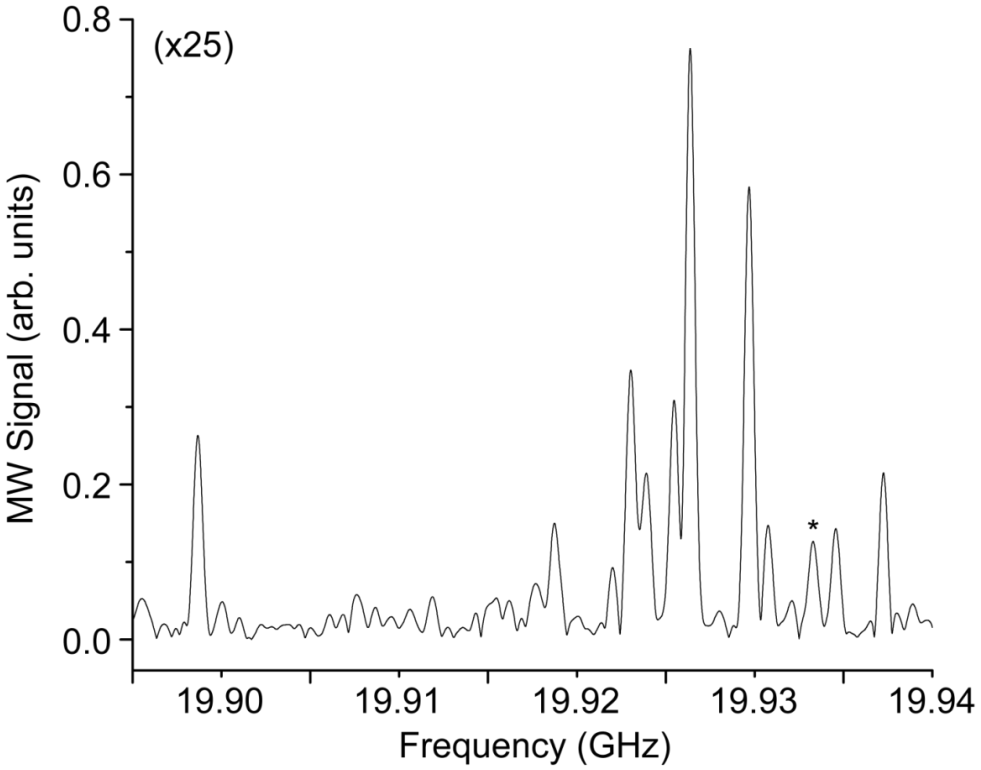

Figure 4.12: Expanded view of the EtSH spectrum. The star indicates a *gauche* 4_{14} (+) ←4_{04} (-) ^{34}S transition at 19938.35 GHz. [5]

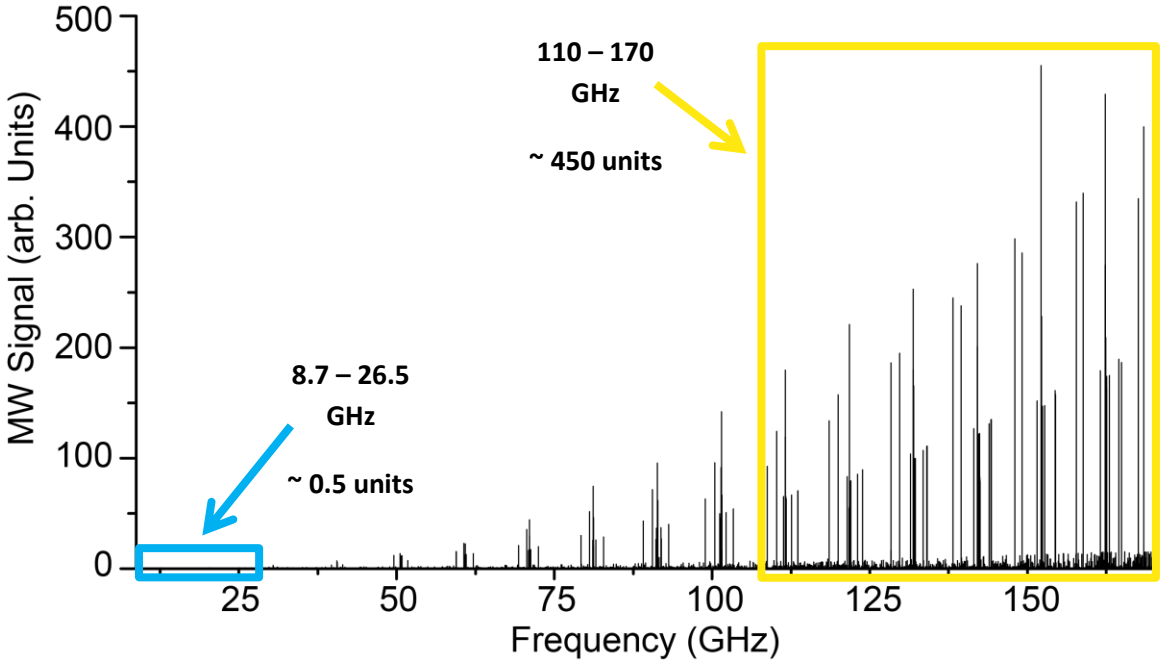

Figure 4.13: The predicted *g*-EtSH spectrum from 8.7 to 170 GHz. The predicted intensity near 170 GHz is ~450 units. The predicted intensity near 26.5 GHz is ~0.5 units and is too low to be seen on the same scale as the 170 GHz data.

5 – 1-Propanethiol

After ethanethiol, 1-propanethiol is the next logical candidate for detection in the ISM. It is very similar to ethanethiol in its composition and behavior, and can be analyzed with a similar Hamiltonian. Like ethanethiol, it is a small slightly asymmetric prolate top with a high vapor pressure and strong dipole moment in each of its conformers. In addition to the thiol *trans* and *gauche* conformers, there are several backbone conformers associated with 1-PrSH. The longer carbon allows for conformerism around the central C-C bond in addition to the C-S bond, which results in 1-PrSH having six possible rotational conformers (Figure 5.1).

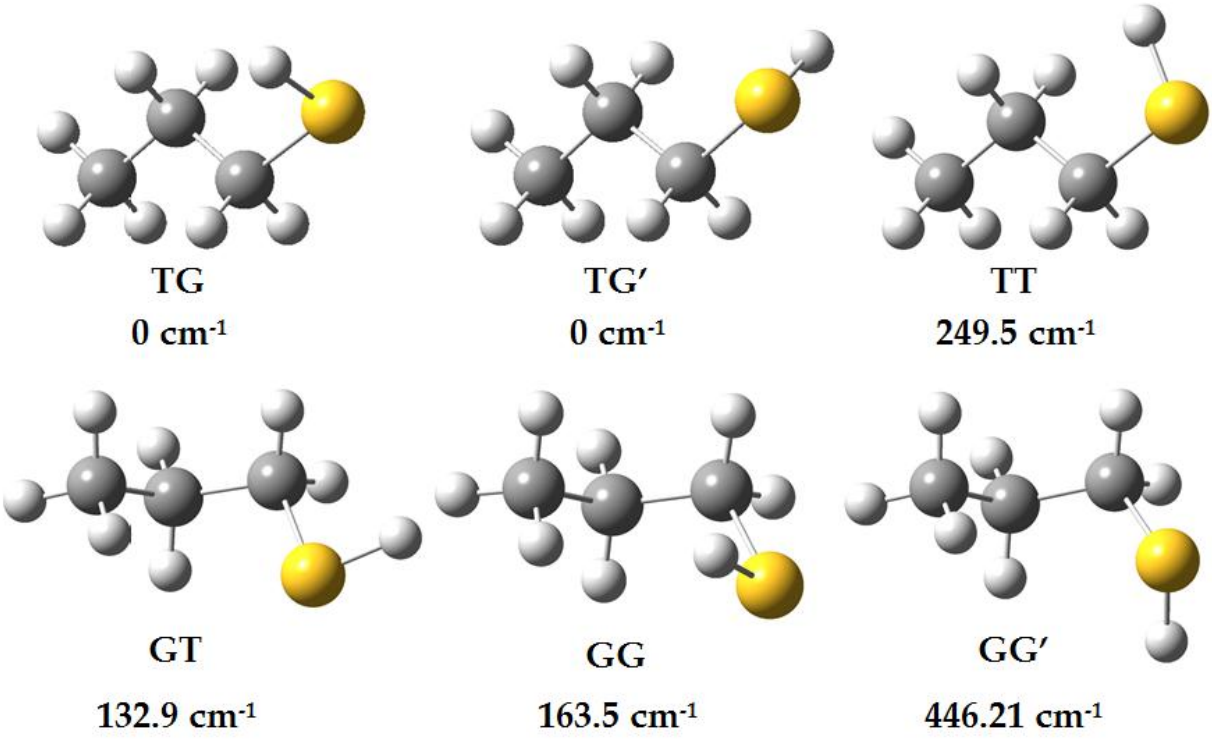

Figure 5.1: The stable conformers of 1-PrSH

The three conformers arising from the *trans* C-C position are the *trans-trans* (TT), the *trans-gauche* (TG), and the *trans-gauche'* (TG'). The other three, *gauche-*

trans (GT), *gauche-gauche* (GG), and *gauche-gauche'* (GG'), are in the *gauche* C-C position. Only the *trans* backbone conformers have been previously studied with rotational spectroscopy. [16], [17]

Each of these conformers contributes to the spectrum of 1-PrSH, making it incredibly dense and challenging to analyze. In addition, 1-PrSH has the highest partition function of the molecules studied in this thesis. This means that the rotational and vibrational energy has more ways to disperse, and so for a fixed number of molecules, all of the observed transitions are less intense.

The spectrum of 1-propanethiol was first studied in 1977 by Ohashi *et al.* with a Stark-modulated spectrometer over the frequency region of 8.4-35 GHz at -40° C. They assigned 33 lines up to J=7 of the ground state normal species of the TG conformer. Additionally, they assigned 34 lines up to J=7 of the v=1 thiol torsion excited state. [17]

Despite the relatively large number of lines fit, their fit was unreliable because they analyzed the spectrum assuming that the TG species was rigid and so they did not incorporate any tunneling factors into their fit. This meant that they were unable to fit any *c*-type transitions. Ohashi *et al.* defended this approach by arguing that no obvious splittings were observed in the vicinity of the rigid rotor predictions. However, the *c*-type transitions are split above and below the rigid rotor predictions by twice the tunneling frequency, on the order of GHz, and so no transitions would be expected to be observed near the rigid rotor predictions, as demonstrated by Schmidt and Nakagawa in their previous work on the *g*-EtSH spectrum.[11][12]

Consequently, Ohashi *et al.* were unable to fit any *c*-type transitions and the *b*-type transitions were also too weak to assign due to the small *b*-dipole moment. They were able to fit the *a*-type transitions, which are only split by a few MHz, by treating them as singlets. They determined the TG-1-PrSH rotational constants to be A = 23429 ± 653, B = 2345.29 ± 0.03, and C = 2250.18 ± 0.03 MHz for the ground state and A = 24483 (934), B = 2346.30 ± 0.04, and C= 2253.91 ± 0.04 MHz for the v=1 thiol torsion excited state. Since their fit only included *a*-type transitions, their A rotational constant could not be well-determined and because of this large uncertainty, these results were not used as a starting point for the present fits.

In 1981, Nakagawa *et al*. published a thorough analysis of both the TT and TG ground state normal species conformers. They chose not to work with any of the *gauche* backbone conformers because they believed that only the TG conformer participated in thiol tunneling because it is the least sterically hindered.[16]

They used a Stark-modulated spectrometer over the frequency region 8.4-34 GHz at 184 K. Using the same Hamiltonian as with EtSH, they were able to assign 69 lines up to J=15 from the TG spectrum. They observed splitting in the *c*-type as well as doublet structure in *a*-type transitions with $K_a = 1$. For the TT conformer, they assigned 26 singlet transitions up to J=10, but reported that many of the TT lines were overlapped by other strong lines, which hampered further progress. The results of their fits are reported in Tables 5.1 and 5.2.

Table 5.1: TG normal species of 1-PrSH			
	Ab Initio [a]	Nakagawa[16]	Observed [b]
A (MHz)	24084.56	23907.47 (9)	23907.68 (33)
B (MHz)	2302.15	2345.597 (6)	2345.61 (286)
C (MHz)	2211.40	2250.338 (9)	2250.32 (272)
Δv (MHz)	-	1613.01 (4)	1613.01 [c]
D± (MHz)	-	1.326 (24)	1.326 [c]
E± (MHz)	-	57.9	53.53 (229)
D_J (MHz)	0.00036	0.00022 (8)	0.00036
D_{JK} (MHz)	-0.00199	-0.0057 (15)	-0.00199
D_K (MHz)	0.059	-	0.059
d_J (MHz)	0.235E-04	-	0.235E-04
d_K (MHz)	0.000927	-	0.000927
Lines Fit	-	69	74
Fit RMS (MHz)	-	0.157	0.123
Max J	-	15	30

a) *Ab initio* values calculated at the B3LYP/6-311++G(d,p) level of theory in Gaussian 09.
b) If no uncertainty reported, then locked to *ab initio* values
c) Locked to previous values from Nakagawa *et al*.

Table 5.2: TT normal species of 1-PrSH			
	Ab Initio [a]	Nakagawa[16]	Observed [b]
A (MHz)	23866.485	23845.24 (22)	23845. 23 (49)
B (MHz)	2319.402	2393.469 (012)	2393.46 (34)
C (MHz)	2200.888	2269.621 (016)	2269.61 (46)
D_J (MHz)	-0.00036	0.51 (14)	-0.00036
D_{JK} (MHz)	0.0019	-	0.0019
D_K (MHz)	-0.055	-	-0.055
d_J (MHz)	-0.2450E-4	-	-0.2450E-4
d_K (MHz)	-0.0003	-	-0.0003
Lines Fit	-	33	26
Fit RMS (MHz)	-	0.04	0.04
Max J	-	10	11

a) *Ab initio* values calculated at the B3LYP/6-311++G(d,p) level of theory in Gaussian 09.
b) If no uncertainty reported, then locked to *ab initio* values
c) Locked to previous values from Nakagawa *et al*.

Before commencing our analysis of the spectrum of 1-PrSH, several *ab initio* calculations were performed on both conformers at the B3LYP/6-311G++ (d,p) level of theory in Gaussian 09. Both the TT and the TG conformers are very similar to their EtSH counterparts. As with EtSH, the TG conformer is more stable than the TT

conformer with an energy difference of 249.5 cm^{-1}. Geometry optimizations indicated that the thiol H-atom is in the plane of symmetry at 180° for the *trans* conformer and is offset from the symmetry plane by 63.11° or -63.11° for the *gauche* and *gauche'* conformers, respectively. The calculations showed that both the TT and TG conformers has strong dipole moments that were in good agreement with the values reported by Nakagawa *et* al.[16] (Tab. 5.3)

Table 5.3: Dipole Moments of 1-PrSH

	Ab Initio *	Nakagawa[16]
TG-1-PrSH		
μ_a (D)	1.70	1.5757 (7)
μ_b (D)	0.027	0.115 (82)
μ_c (D)	0.71	0.580 (9)
μ_{total} (D)	1.84	1.683 (10)
TT-1-PrSH		
μ_a (D)	1.25	1.179 (18)
μ_b (D)	1.24	1.078 (75)
μ_c (D)	0.0	0
μ_{total} (D)	1.76	1.598 (54)

*Calculated at the B3LYP/6-311++G(d,p) level of theory in Gaussian 09.

1D potential energy scans were performed on the methyl rotor dihedral and the thiol rotor dihedral. Each calculation scanned the potential energy over 360° about the dihedral angle in a series of 36 steps of 10°. The methyl dihedral scans (Fig.5.2) were fit to a V_3 potential and the thiol dihedral scan (Fig. 5.3) was fit to a V_2 + V_3 potential. The results of those scans are listed in Table 5.4.

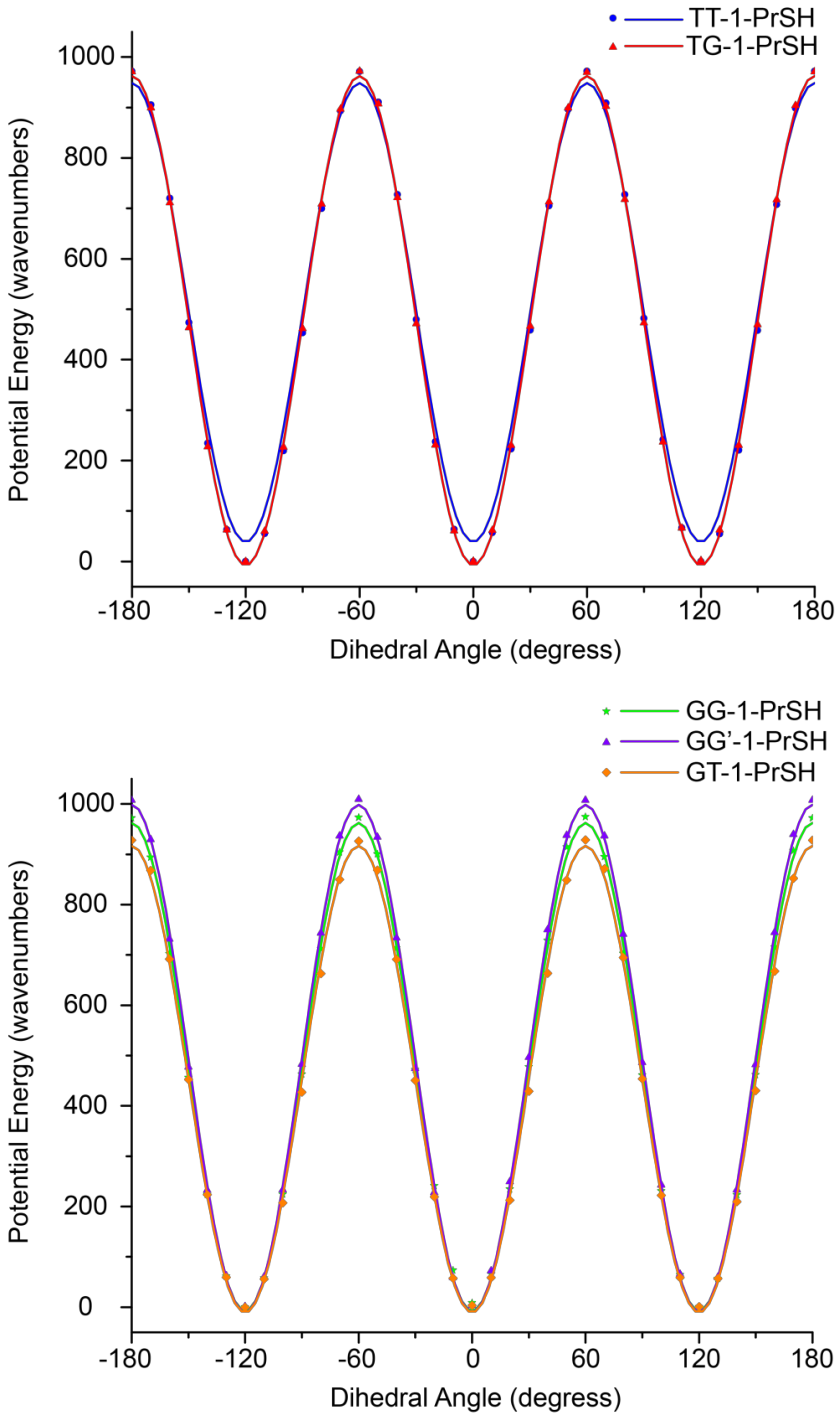

Figure 5.2: Methyl torsion dihedral scan angle results from a 1D potential energy scan of TG-1-PrSH and TT-1-PrSH (top) and GG-1-PrSH, GG'-1-PrSH, GT-1-PrSH (bottom) at the B3LYP/6-311G+(d,p) level of theory in Gaussian 09. In each graph, the symbols are the calculated points and the line is the V_3 potential energy fit.

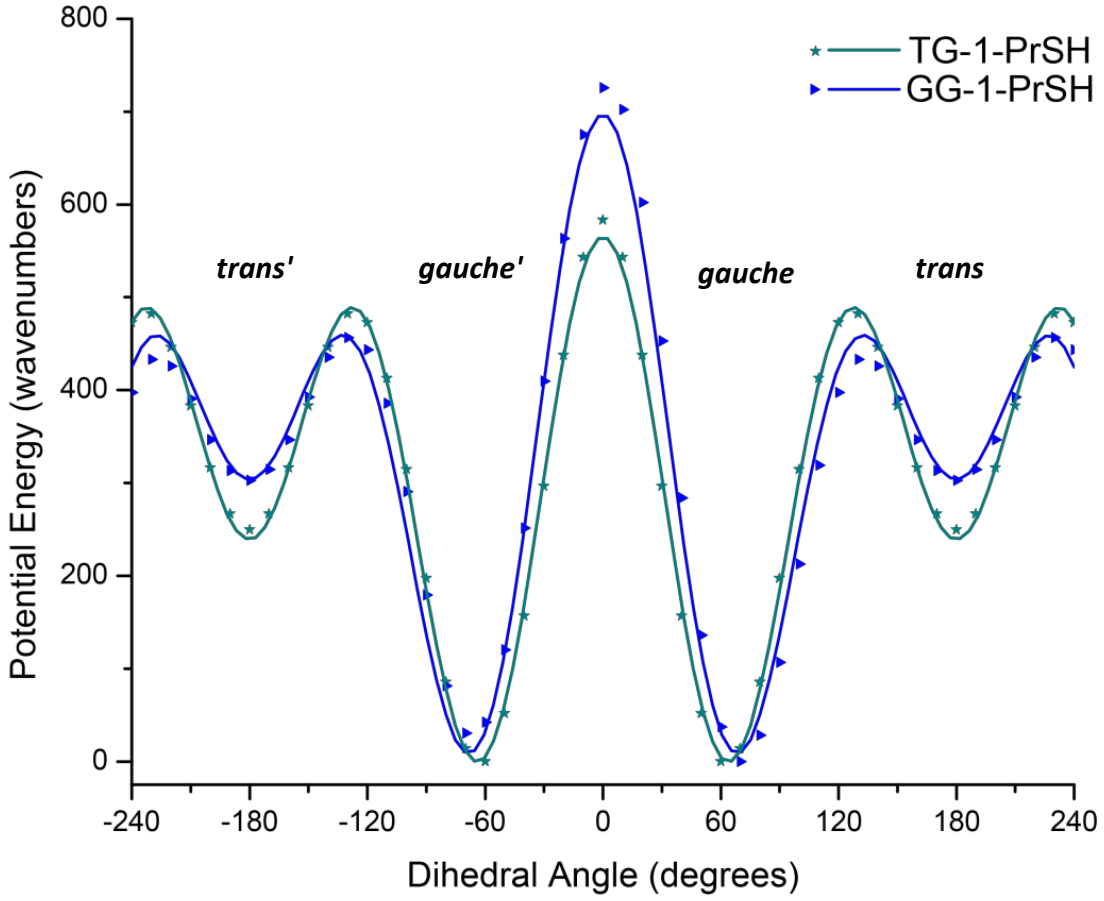

Figure 5.3: Thiol torsion dihedral scan angle results from a 1D potential energy scan of TG-1-PrSH and GG-1-PrSH at the B3LYP/6-311G+(d,p) level of theory in Gaussian 09. In each graph, the symbols are the calculated points and the line is the V_3 potential energy fit.

Table 5.4: *Ab Initio Relative Energy Simulations**					
Thiol Torsion Fits (cm^{-1})					
	Previous *trans* backbone[16]	*trans* backbone*	*gauche* backbone*		
V_2	-123.5 (6)	-191.4 (20.4)	-374.06 (10.2)		
V_3	458.2 (9)	428.92 (18.6)	401.2 (9.6)		
Methyl Torsion Fits (cm^{-1})*					
	TG	TT	GG	GG'	GT
V_3	969.27 (3.5)	972.87 (5.2)	968.91 (5.1)	1007.31 (4.5)	925.83 (5.9)

*Calculated at the B3LYP/6-311++G(d,p) level of theory in Gaussian 09.

Like the *trans* conformer in EtSH, TT-1-PrSH has no *c*-dipole moment because the thiol H-atom is in the symmetry plane. The methyl group is slightly less hindered than in EtSH but as shown in the potential energy scan in Figure 5.2, the barrier to internal rotation for the methyl rotor is sufficiently high that transitions arising from TT-1-PrSH are predicted to be observed as singlets at our current spectral resolution.

The TG spectrum of 1-PrSH is very similar to the spectrum of *g*-EtSH. The thiol H-atom is offset from the plane of symmetry, producing TG and TG' mirror images, and it can tunnel through the barrier to convert between the two forms. The potential energy scan in Figure 5.3 shows that the V_3 barrier to the thiol rotation is 428.92 ± 18.6 cm^{-1}, which is lower than the 451.68 ± 17 cm^{-1} barrier of *g*-EtSH.

Anharmonic frequency calculations in the center of mass frame of reference provided anharmonically corrected vibrational frequencies and vibration- rotation coupling constants for the v=1 excited states. The first five excited states are listed in Table 5.5 for the TG and TT conformers and in table 5.6 for the GG, GG', and GT conformers.

Table 5.5: Calculated[a] vibrational energies, relative intensities and rotation-vibration coupling constants for the *trans* backbone conformers of 1-PrSH					
Description	**ΔE (cm^{-1})[b]**	**Pred. Int. (250 K)[c]**	**α_A (MHz)**	**α_B (MHz)**	**α_C (MHz)**
TG					
Ground State	0	1	-	-	-
Twist (Asymmetric)	113.05	0.52	511.58	-1.23	-3.98
Methyl-Thiol torsion (Asym)	193.72	0.33	-33.20	2.91	3.10
Methyl torsion	232.99	0.26	-243.29	0.66	1.58
Methyl-Thiol torsion (Sym)	248.38	0.24	-201.92	1.59	1.74
Backbone bend (Sym)	359.21	0.13	-38.68	2.14	2.59
TT					
Ground State	249.52	0.12	-	-	-
Twist (Asymmetric)	348.27	0.067	439.19	-2.15	-5.67
Methyl-Thiol torsion (Asym)	408.96	0.048	201.74	7.87	3.13
Methyl torsion	474.40	0.033	-468.97	-1.23	1.44
Methyl-Thiol torsion (Sym)	492.231	0.029	-42.82	2.52	1.65
Backbone bend (Sym)	599.74	0.016	-56.84	1.86	2.48

a) Calculated at the B3LYP/6-311++G(d,p) level of theory in Gaussian 09.

b) Not zero-point corrected. Scaled using the ground state TG-1-PrSH as a zero

c) Includes two-fold degeneracy of TG conformer

The anharmonic calculations also predicted the dipole moments as well as the rotational and distortion constants for each conformer. The *ab initio* dipole moments of the TT and TG conformers were reported earlier in Table 5.3. The rotational and distortion constants for TT- and TG-1-PrSH are in Tables 5.1 and 5.2 for the *gauche* and *trans* conformers, respectively. The *ab initio* dipole moments of the GG, GG', and GT conformers are listed in Table 5.7, as well their rotational and distortion constants.

Table 5.6: Calculated[a] vibrational energies, relative intensities and rotation-vibration coupling constants for the *gauche* backbone conformers of 1-PrSH					
Description	**ΔE (cm^{-1})[b]**	**Pred. Int. (250 K)[c]**	**α_A (MHz)**	**α_B (MHz)**	**α_C (MHz)**
GG					
Ground State	132.91	0.23	-	-	-
Twist (Asymmetric)	261.75	0.11	-53.98	7.50	5.09
Methyl-Thiol torsion (Sym)	321.08	0.079	4.32	-4.31	-0.24
Methyl-Thiol torsion (Asym)	339.71	0.071	-31.10	6.73	6.41
Backbone twist	424.11	0.04	50.92	-3.47	0.44
Backbone bend (Sym)	555.61	0.02	-47.71	10.00	6.92
GG'					
Ground State	163.48	0.20	-	-	-
Twist (Asymmetric)	280.33	0.10	-55.75	5.48	2.83
Methyl-Thiol torsion (Sym)	363.70	0.062	67.09	-15.56	-8.05
Methyl-Thiol torsion (Asym)	383.118	0.055	-59.97	12.33	7.88
Backbone twist	462.75	0.035	62.24	-4.32	-0.96
Backbone bend (Sym)	574.928	0.018	-61.00	10.55	6.77
GT					
Ground State	446.21	0.038	-	-	-
Twist	532.73	0.023	-116.26	39.14	8.07
Thiol torsion	600.22	0.016	-33.51	16.60	10.45
Methyl torsion	655.67	0.011	-44.97	10.66	6.43
Backbone bend (Rock)	736.18	0.0072	47.30	-0.95	0.97
Backbone bend (Sym)	849.63	0.0038	-52.06	9.95	6.05

a.) Calculated at the B3LYP/6-311++G(d,p) level of theory in Gaussian 09.

b.) Not zero-point corrected. Scaled using the ground state TG-1-PrSH as a zero

c.) Includes two-fold degeneracy of TG conformer

Table 5.7: *Ab Initio* Calculations* for the 1-PrSH *gauche* backbone conformers			
	GG	GG'	GT
μ_a (D)	1.272	1.648	0.736
μ_b (D)	1.107	0.328	1.440
μ_c (D)	0.554	0.649	0.633
μ_{total} (D)	1.775	1.802	1.737
A (MHz)	11608.686	11699.682	11518.757
B (MHz)	3107.784	3110.983	3211.786
C (MHz)	2729.124	2699.645	2768.402
D_J (MHz)	0.001983	0.002104	0.002904
D_{JK} (MHz)	0.01051	0.01223	0.05821
D_K (MHz)	-0.04744	-0.05481	-0.01577
d_J (MHz)	0.0004667	0.0005218	0.0008456
d_K (MHz)	0.005464	0.006010	0.01089

*Calculated at the B3LYP/6-311++G(d,p) level of theory in Gaussian 09.

We measured the spectrum of 1-PrSH (Figure 5.4) from 8.7 to 26.5 GHz at 251 K and 7 mTorr. Two million averages were collected across the full bandwidth, as well as a blank at high pressure that was subtracted from the data set. The collected spectrum is dense and complicated due to the large number of conformers and vibrational states present at ~251 K..

For both TT- and TG-1-PrSH, we began our analysis of with a combination of the rotational constants from Nakagawa *et al.*[16] and the distortion constants from *ab initio* calculations. Out of 908 lines in the spectrum in total, 100 lines were assigned to the ground state normal species. This includes 26 lines up to J=15 to the TT conformer and 74 lines up to J=30 to the TG conformer. The observed constants for the TG- and TT-1-PrSH fits were reported previously in Tables 5.1 and 5.2, respectively.

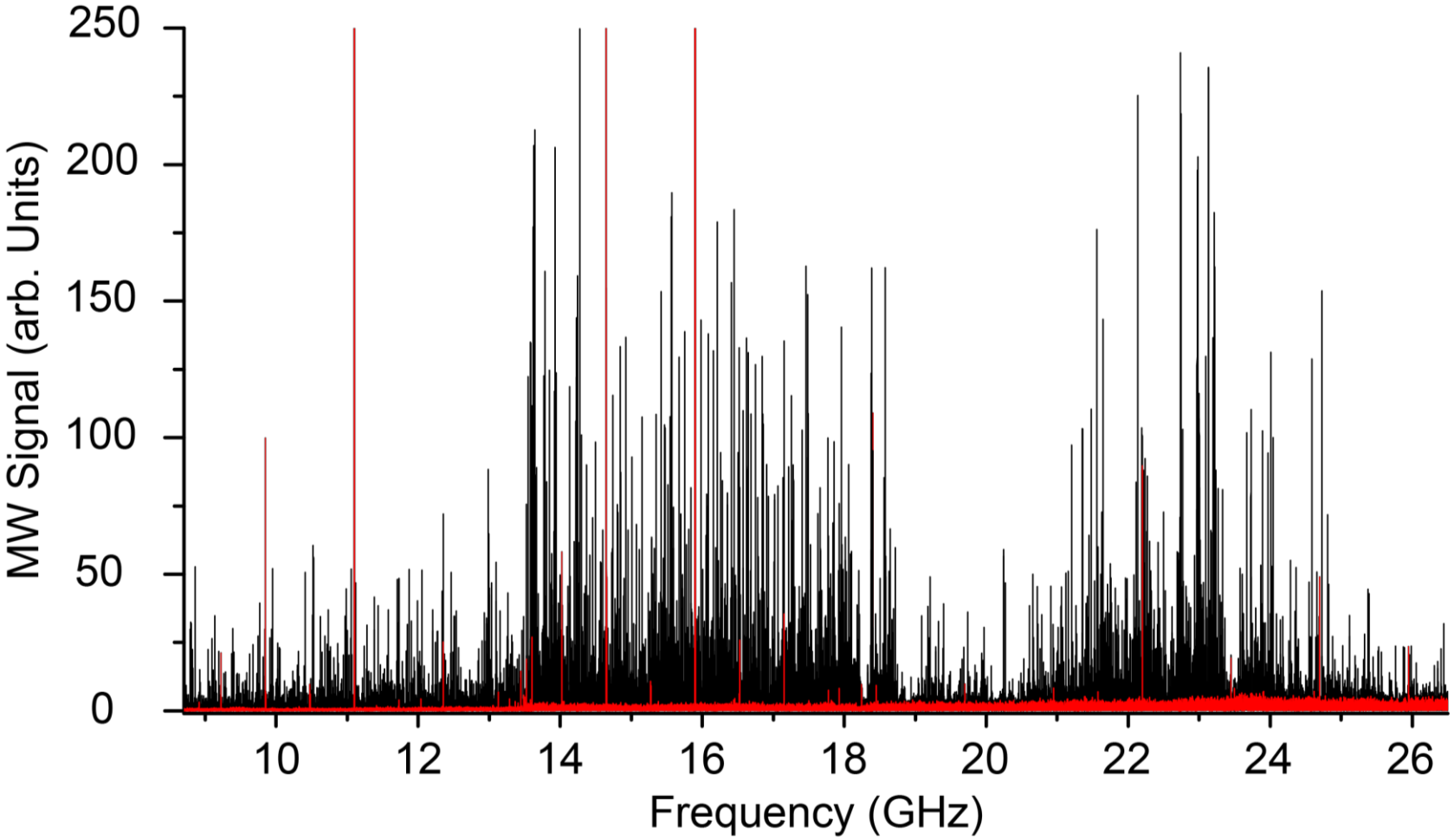

Figure 5.4: The spectrum of 1-PrSH from 8.7 to 26.5 GHz at ~251 K and 7 mTorr, with a 4 μs FID and 2 million averages. At this scale, there are 908 peaks above the 3:1 signal to noise cutoff at 5 units. Many of the transitions are due to molecules in excited vibrational states.

Using the same Hamiltonian that was used for *g*-EtSH, the TG-1-PrSH spectrum was able to be fit using SPFIT/SPCAT. Large tunneling splittings of ~3200 MHz were observed in the *c*-type transitions. The tunneling frequency, Δv, was fit to be 1613.01 ± 4 MHz. The parameter E± was determined to be 53.53 (229) MHz. Figure 5.5 shows expanded views of the 1-PrSH data (black) against the predicted spectrum TG conformers (red) on the negative scale generated from our experimental constants. It can be seen that the predicted peaks are within the tens of KHz. The entire predicted *gauche* (red) spectra can be seen for each of the lower, middle and upper band circuits in Figures 5.6, 5.7, and 5.8.

The *trans* conformer could be predicted using the Watson A-Reduced Hamiltonian, but was much less intense than *gauche* conformer. Numerous TT-1-PrSH transitions were overlapped by stronger lines or in the noise and many of the stronger transitions were above our frequency range. Our fit of TT-1-PrSH was as well determined as the previous work,[16] but were unable to improve it. 26 lines were fit to J=11, but this was only 1 greater J=10 max J reported by Nakagawa *et al*.[16] Thus, the TT conformers fits are not being displayed.

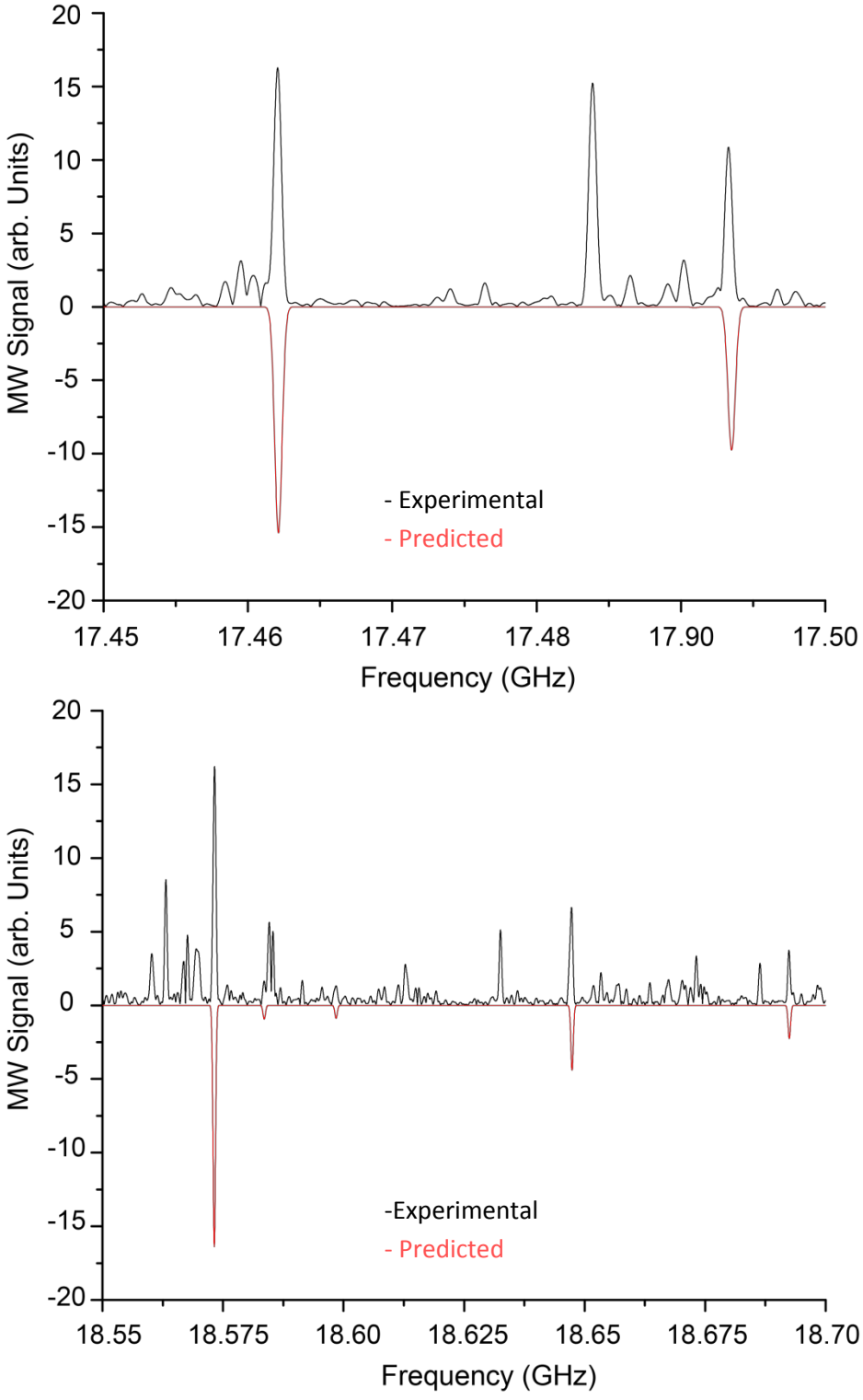

Figure 5.5: Expanded view of the experimental spectrum of1-PrSH (black) versus simulated data from the experimental TG conformer rotational constants on the negative scale (red).

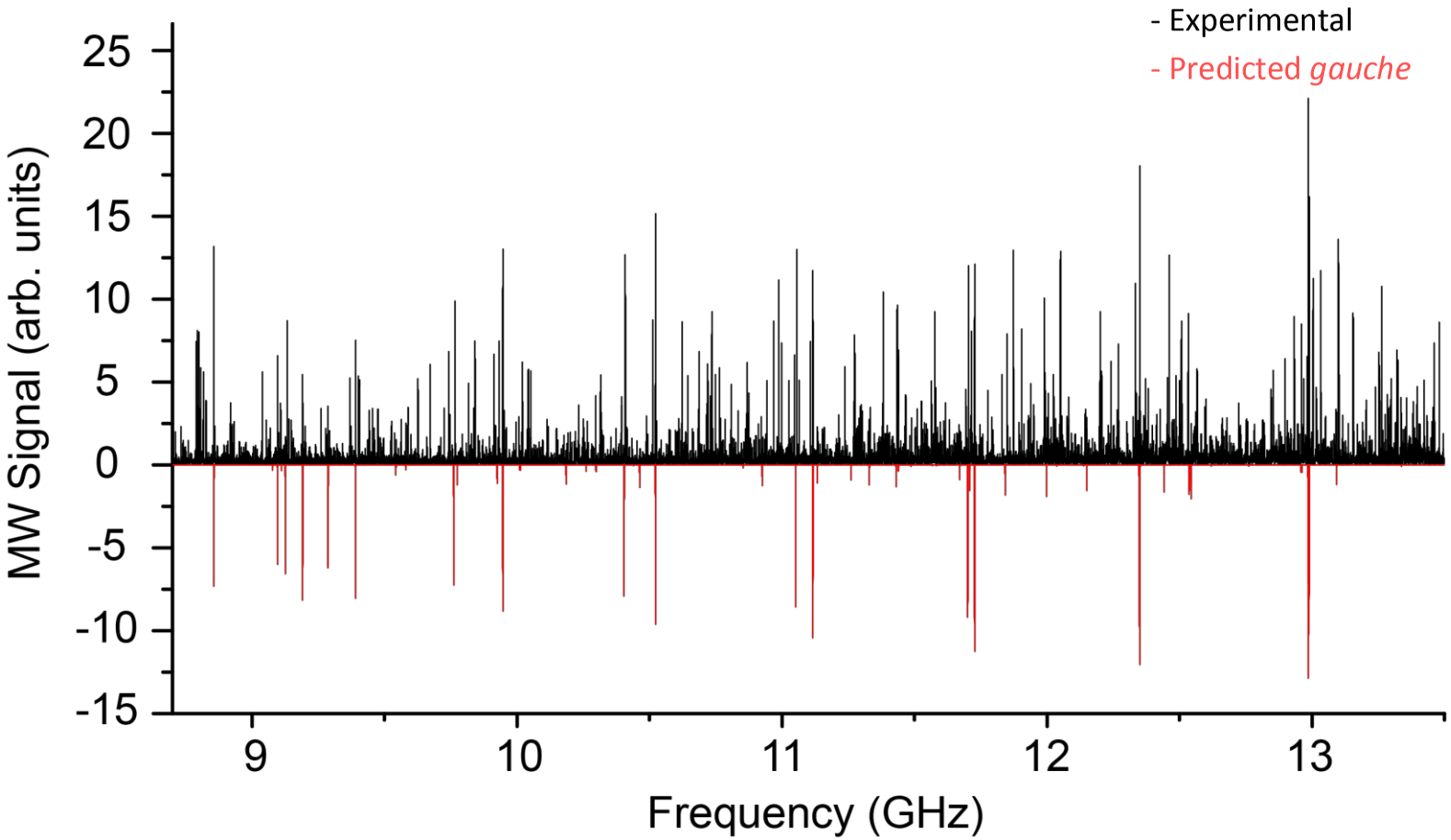

Figure 5.6: Experimental spectrum of 1-PrSH from 8.7 to 13.5 GHz against simulated data from the experimental rotational constants on the negative scale. The predicted TG is simulated in red.

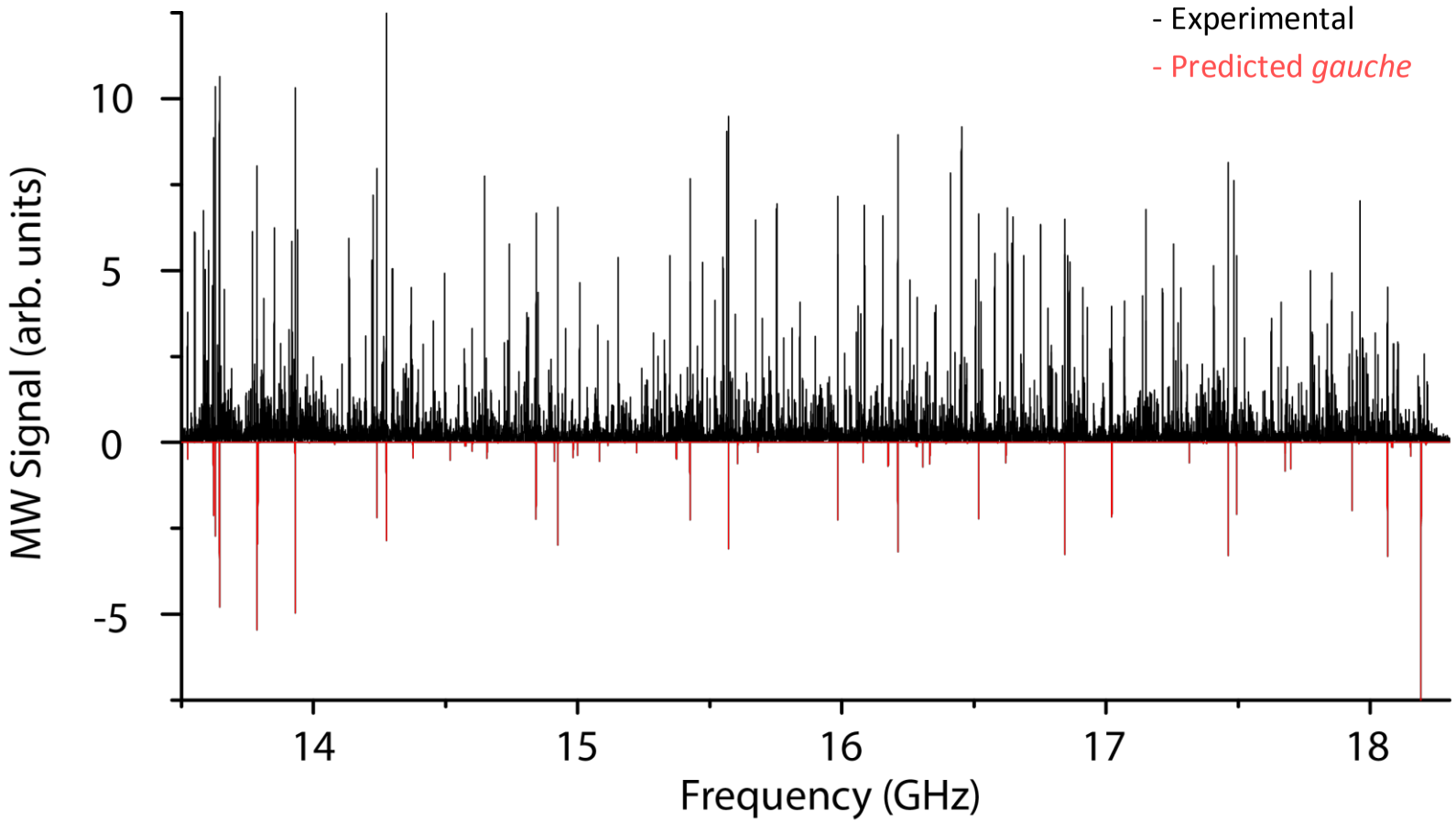

Figure 5.6 Experimental spectrum of 1-PrSH from 13.5 to18.3 GHz against simulated data from the experimental rotational constants on the negative scale. The predicted TG is spectrum simulated in red.

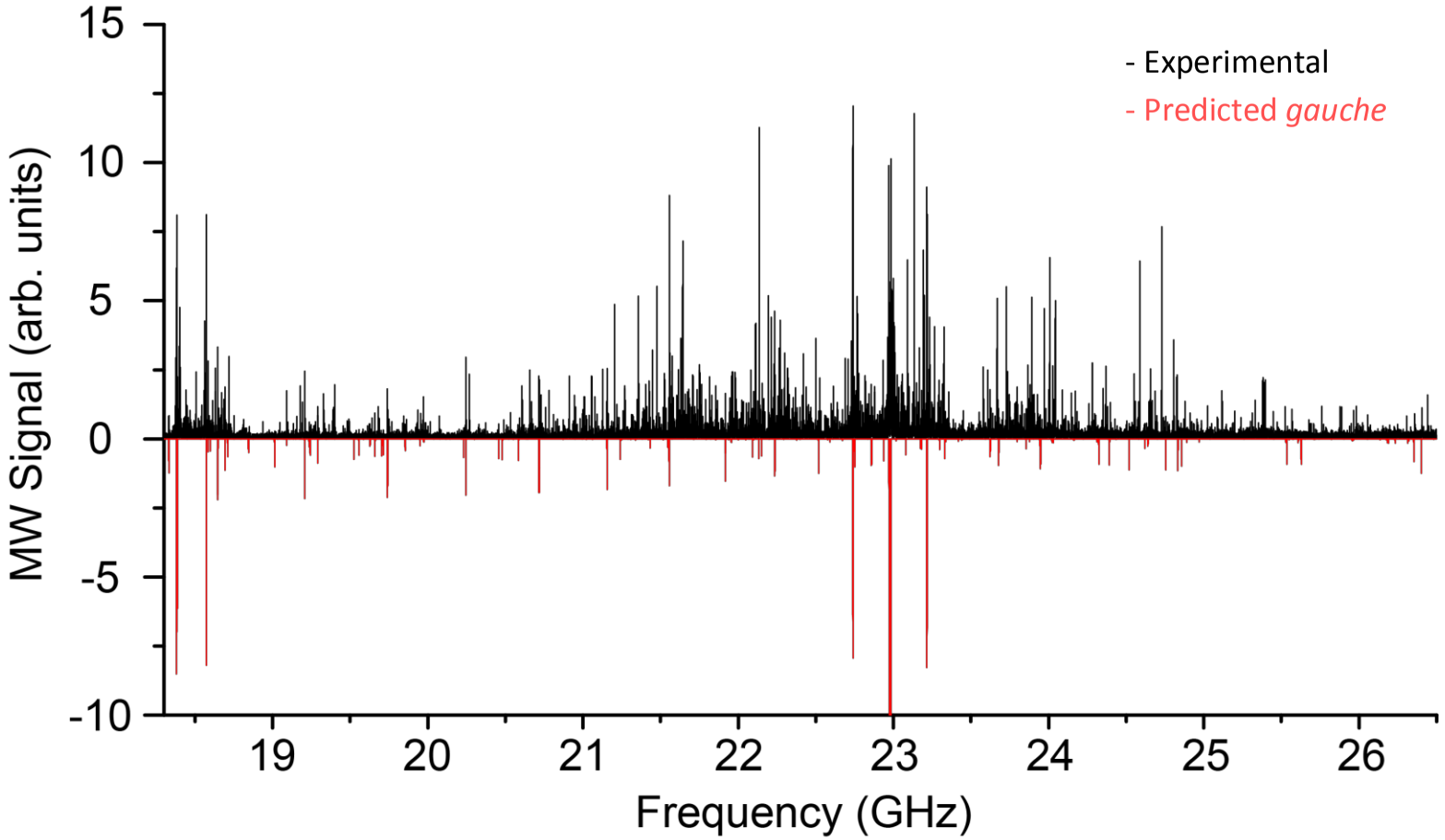

Figure 5.8: Experimental spectrum of 1-PrSH from 18.3 to 26.5 GHz against simulated data from the experimental rotational constants on the negative scale. The predicted TG is spectrum simulated in red.

Only one of the five stable conformers has been successfully fit, so there is still much more work to do on 1-PrSH. From here, the next step is to develop a Hamiltonian for the GG and GG' conformers, which are more abundant than the TT conformers, as can be seen in Table 5.6. The thiol dihedral scan (Fig. 5.3) for GG- and GG'-1-PrSH torsion is similar to the scan of the TG-and TG'-1-PrSH torsion, so it is reasonable to assume that tunneling interactions are also present in GG- and GG'-1-PrSH conformers. The *gauche* backbone conformers offer an additional challenge because all three conformers are completely asymmetric and have no mirror plane Therefore, more than one of the *a-, b-,* and *c*-dipoles may be involved in the tunneling splitting.

There are also several excited vibrational states at appreciable intensities (Tables 5.5 and 5.6) that require attention as well. Two stable conformers and 3 TG-1-PrSH excited states that are calculated to be more abundant than the TT-conformer. Additionally, once we have fit these conformers, the lines from their spectra can be cut from the data. Then just the residuals remain which reduces the possibility of false positives, which are problematic in crowded spectra like the ones in this thesis.

6) 2-Propanethiol

Like the previous two molecules discussed in this thesis, 2-propanethiol (2-PrSH) is also a reasonable candidate for detection in the ISM. It is a prolate asymmetric rotor with a high vapor pressure and strong dipole moment. It has two conformers, the *trans* and the *gauche* (Fig. 6.1), and *ab initio* calculations show that the *trans* conformer is more stable by 41.3 cm^{-1}.

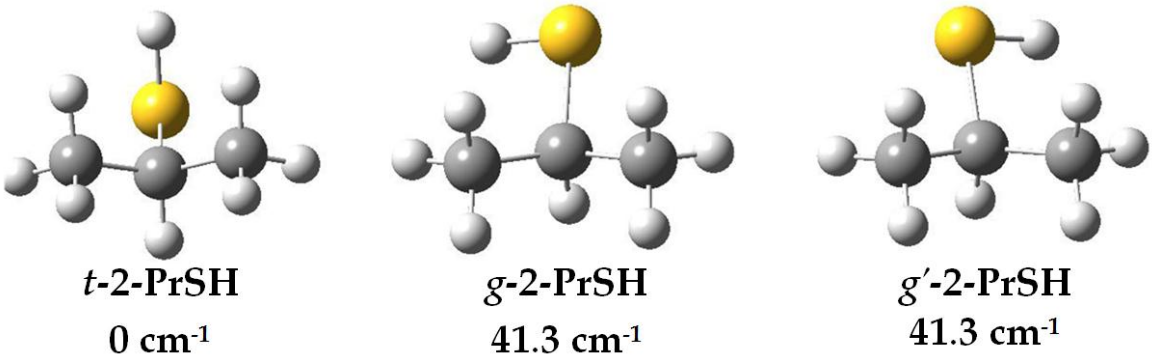

Figure 6.1: The stable conformers of 2-PrSH

The microwave spectrum of 2-propanethiol has been previously analyzed by Griffiths *et al.* in 1975.[18] They used a Stark-modulated spectrometer between 12 and 40 GHz. Their work included both the *trans* and *gauche* conformers and they performed double resonance experiments to confirm their assignments.

For the ground state normal species they assigned 12 lines up to J = 4 for the *trans* conformer and 20 lines up to J = 4 for the *gauche* conformer. They were able to easily assign *a*-type transitions for the *trans* conformer, but no *c*-type transitions were fit because the weak *c*-dipole lines could not be seen in the dense spectrum. Since their fit was only calculated from *a*-type parameters, their A rotational constant was the least well defined.

Griffiths *et al*. reported that the *b*-dipole transitions were split above and below their rigid rotor predictions due to the thiol H interconverting between the *g*-2-PrSH and *g'*-2-PrSH conformers.

While Griffiths *et al*. claim to have accounted for this in their analysis, they did not report their Hamiltonian, only claiming that it was similar to that of Meakin and Hirota *et al*.[19] Their fits are further occluded by the fact that they wrote that they used nine parameters to fit their transitions, only reported six parameters. It appears as though they allowed the six symmetric and antisymmetric rotational constants (A_+, B_+, C_+ and A_-, B_-, C_-) to float separately and then averaged them later to get three. The rotational constants should be locked to each other because the splitting is determined by other terms in the Hamiltonian. Allowing the rotational constants to vary will let the fit compensate for poorly determined tunneling parameters, but the improvement to the fit is artificial. Hence, their experimental values are not well determined.

Like the previous two molecules, *g*-2-PrSH exhibits tunneling interactions about the mirror plane between the *gauche* and *gauche'* conformers. Unlike *g*-EtSH and TG-1-PrSH, now the *b*-dipole transitions are split by twice the tunneling frequency. These splittings also cannot be predicted using the Watson A-Reduced Hamiltonian, so a more complete Hamiltonian is need. Since we were unable to determine the Hamiltonian used by Griffiths *et al*., we used a new Hamiltonian based on later work by Hirota *et al.* on isopropyl alcohol[20] and incorporated the quartic distortion constants from the Watson A-Reduced Hamiltonian. The terms of the resulting Hamiltonian, which can be seen below, are explained in Table 6.1.

$$\hat{H} = \hat{H}_{++} + \hat{H}_{--} + \hat{H}_{+-} + \hat{H}_d^{\{4\}} \quad (6.1)$$

$$\hat{H}_{++} = A_+ \hat{J}_a^2 + B_+ \hat{J}_b^2 + C_+ \hat{J}_c^2 \quad (6.2)$$

$$\hat{H}_{--} = A_- \hat{J}_a^2 + B_- \hat{J}_b^2 + C_- \hat{J}_c^2 + \Delta\nu \quad (6.3)$$

$$\hat{H}_{+-} = G_a (i\hat{J}_a) + G_c (i\hat{J}_c) + F_c (P_a \hat{J}_b + P_b \hat{J}_a) + F_a (P_b \hat{J}_c + P_c \hat{J}_b) \quad (6.4)$$

$$\hat{H}_d^{\{4\}} = -D_J \hat{J}^4 - D_{JK} \hat{J}^2 \hat{J}_c^2 - D_K \hat{J}_c^4 - 2d_J \hat{J}^2 (\hat{J}_a^2 - \hat{J}_b^2) - d_K [\hat{J}_c^2 (\hat{J}_a^2 - \hat{J}_b^2) + (\hat{J}_a^2 - \hat{J}_b^2) \hat{J}_c^2] \quad (6.5)$$

Table 6.1: Terms of the *g*-2-PrSH Hamiltonian

Symmetric state (+) rotational constants	Antisymmetric state (-) rotational constants	Cross Terms connecting the (+) and (-) states	Energy separation of (+) and (-) states	Operators
A_+	A_-	G_a		$(\hat{J}_a\hat{J}_b + \hat{J}_b\hat{J}_a)$
B_+	B_-	G_c	$\Delta\nu$	$(\hat{J}_a\hat{J}_b + \hat{J}_c\hat{J}_b)$
C_+	C_-	F_c		$\hat{J}_a^2$, $\hat{J}_b^2$, and $\hat{J}_c^2$
		F_a		

The selection rules for the *g*-2-PrSH conformer are that *a*- and *c*-type transitions are allowed between two symmetric states or two antisymmetric states (+ ↔ + and – ↔ –) while *b*-type transitions only connect symmetric and antisymmetric states (+ ↔ –).

Ab initio geometry optimizations were performed on both conformers at the B3LYP/6-311G ++ (d,p) level of theory in Gaussian 09. The *trans* conformer was calculated to be more stable by 41.3 cm^{-1} (Table 6.2). However, the *gauche* conformer is still the more abundant conformer due to its two fold degeneracy and has been calculated to be 1.58 times as intense as the *trans* conformer.

The ground state and first five anharmonically corrected vibrational frequencies, relative energies, relative abundances, and rotational- vibrational coupling constants for the v=1 excited states are listed in Table 6.2. All of the relative intensities are scaled to account for degeneracy of *g*-EtSH, as well.

Table 6.2: Calculated[a] vibrational energies, relative intensities and rotation-vibration coupling constants for 2-PrSH

Description	ΔE (cm^{-1})[b]	Pred. Int. (250 K)[c]	α_A (MHz)	α_B (MHz)	α_C (MHz)
***t*-2-PrSh**					
Ground State	0	1	-	-	-
Thiol torsion	212.19	0.295	-0.2805	-2.5528	4.6961
Methyl torsion (Asym)	267.19	0.215	9.5369	4.8598	3.9013
Methyl torsion (Sym)	287.36	0.191	25.3604	4.7236	4.4173
C-S Rock	327.60	0.152	-23.5977	2.7334	38.7711
Backbone Scissor	414.69	0.092	-2.17412	-4.2651	-32.4261
***g*-2-PrSH**					
Ground State	41.32	1.58	-	-	-
Thiol torsion	235.05	0.52	-0.0608	18.7633	4.3435
Methyl torsion (Asym)	306.71	0.34	12.7680	8.1279	4.3664
Methyl torsion (Sym)	325.62	0.31	31.5172	7.17480	6.7849
C-S Rock	342.55	0.28	-37.6820	-0.6037	14.4517
Backbone Scissor	458.46	0.14	-2.30946	-4.1715	-10.3023

a) Calculated at the B3LYP/6-311++G(d,p) level of theory in Gaussian 09.
b) Not zero-point corrected. Scaled using the ground state TG-1-PrSH as a zero
c) Includes two-fold degeneracy of TG conformer

1D potential energies scans for the methyl rotor dihedral and the of the thiol rotor dihedral were performed on the optimized *trans* and *gauche* structures. The potential energy of each rotor was scanned over 360° about the dihedral angle in a series of 36 steps of 10°. The thiol dihedral scan (Fig. 6.2) was fit to a $V_2 + V_3$ potential the methyl dihedral scans (Fig.6.3) were fit to a V_3 potential. The results of those scans are listed in Tables 6.3.

Table 6.3: *Ab Initio* Relative Energy Simulations		
	Previous TG[1]	*Ab Initio**
Thiol Torsion Fits (cm^{-1})		
V_2	-	47.74 (14.4)
V_3	657.54	489.44 (13.4)
Methyl Torsion Fits (cm^{-1}) *		
	trans	*gauche*
V_3	1309.55 (8.0)	1188.30 (6.9)

*Calculated at the B3LYP/6-311++G(d,p) level of theory in Gaussian 09.

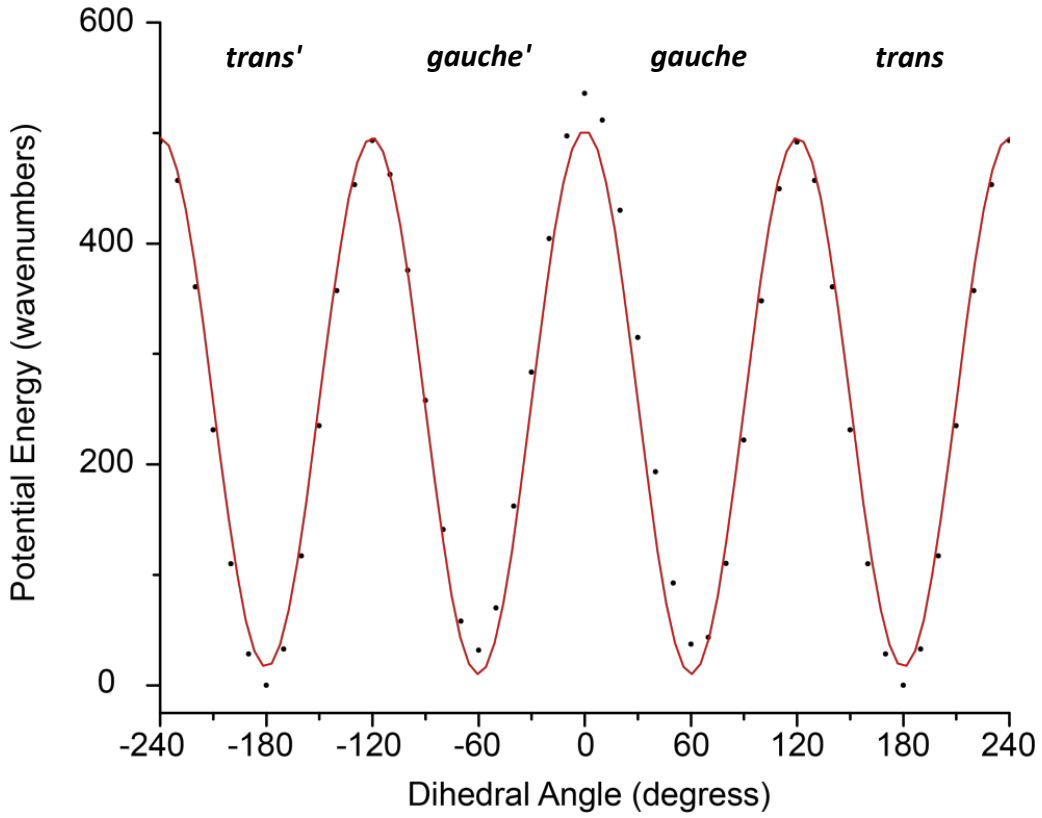

Figure 6.2: Thiol torsion dihedral scan angle results from a 1D potential energy scan of 2-PrSH at the B3LYP/6-311++G(d,p) level of theory in Gaussian 09

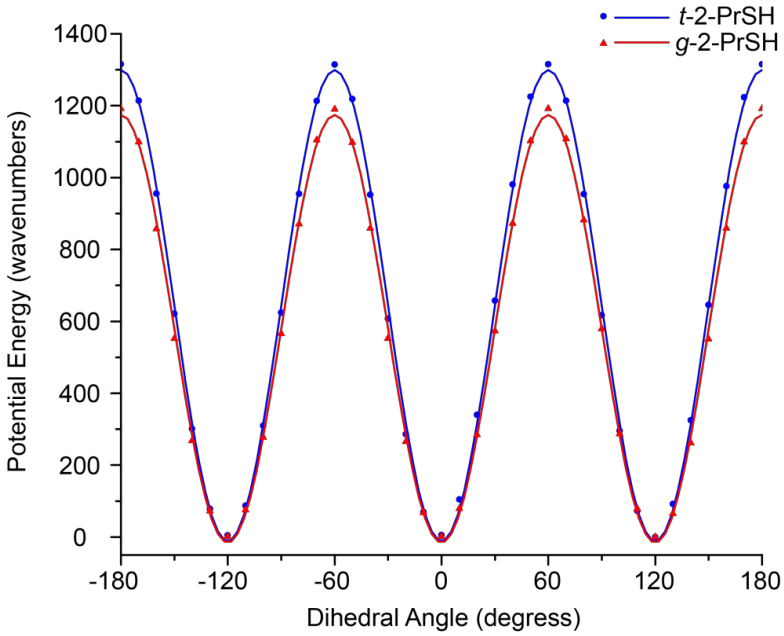

Figure 6.3: Methyl torsion dihedral scan angle results from a 1D potential energy scan of *t*-2-PrSH and *g*-2-PrSH at the B3LYP/6-311++G(d,p) level of theory in Gaussian 09.

Ab initio values for the dipole moments, rotational constants, and distortion constants for were calculated for each conformer. *Ab initio* dipole moments are listed in Table 6.4. The rotational and distortion constants are listed in Tables 6.5 and 6.6 for the *trans and gauche* conformers, respectively.

Table 6.4: Dipole Moments for 2-PrSH		
	*Ab Initio**	Griffiths [18]
t-2-PrSH		
μ_a (D)	1.75	1.59 ± 0.004
μ_b (D)	0.004	0 (assumed)
μ_c (D)	0.38	0.24 ± 0.009
μ_{total} (D)	1.80	1.61 ± 0.2 D
g-2-PrSH		
μ_a (D)	1.52	1.376
μ_b (D)	0.70	0.490
μ_c (D)	0.70	0.463
μ_{total} (D)	1.81	1.53 (20)

*Calculated at the B3LYP/6-311++G(d,p) level of theory in Gaussian 09.

The spectrum of 2-propanethiol was collected from 8.7 to 26.5 GHz at ~251K and 6 mTorr. We collected 2 million averages across the full bandwidth, along with a high pressure blank. The full spectrum can be seen in Figure 6.4 with the blank overlaid in red. The spectrum of 2-PrSH is very crowded due to the large number of conformers and vibrational states present at ~251 K.

Out of 964 lines above the 3:1 noise threshold, 61 were assigned up to J=66. All of the assigned lines were due to the *trans* conformer. Work has been done on the *gauche* conformer yet. The *ab initio* and literature values for *g*-2-PrSH are listed in Table 6.5.

Table 6.5: gauche normal species of 2-PrSH

	*Ab Initio**	Griffiths[18]
A (MHz)	7822.81	7880.13 (103)
B (MHz)	4417.69	4524.60 (02)
C (MHz)	3106.01	3169.36 (47)
Δv (MHz)	-	562.38
Ga (MHz)	-	24.97 (07)
Gc (MHz)	-	15.98 (0.10)
D± (MHz)	-	-
E± (MHz)	-	-
D_J (MHz)	0.0015	-
D_{JK} (MHz)	0.0024	-
D_K (MHz)	0.0026	-
d_J (MHz)	0.00044	-
d_K (MHz)	0.0033	-
Lines Fit	-	-
Fit RMS (MHz)	-	-
Max J	-	-

Calculated at the B3LYP/6-311++G (d,p) level of theory in Gaussian 09.

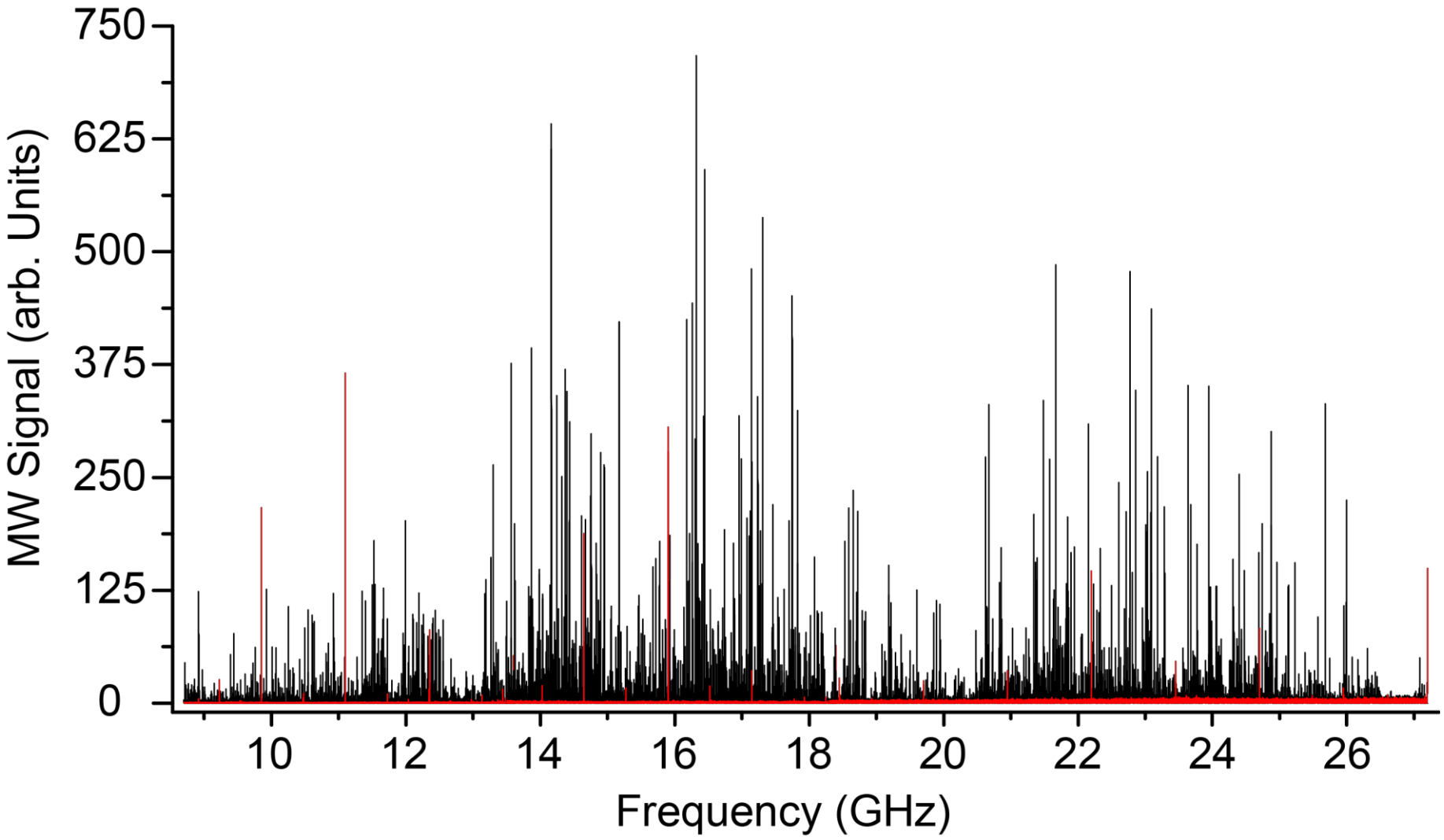

Figure 6.4: Full spectrum of 2-PrSH from 8.7 to 26.5 GHz (black) at 251 K, 6 mTorr, and 2 million averages. The noise level (red) is at 7.5 intensity units. There are 964 peaks above the 3:1 signal-to-noise cutoff.

We began our analysis on the *trans* conformer using the rotational constants from Griffiths *et al.*[1] and the distortion constants from *ab initio* calculations (Table 6.4). The spectra of the *trans* conformer could be predicted using Watson A-Reduced Hamiltonian. Even though it is less abundant, than the *gauche* conformer, many strong transitions were fit to *t*-2-PrSH.

The quality of the *t*-2-PrSHfit can be seen in Figure 6.5 which shows expanded views of the experimental data (black) against the predicted *trans* spectrum (blue) on the negative scale generated from our experimental constants. The full predicted *trans* (blue) spectrum can be seen for each of the frequency regions in Figures 6.6, 6.7, and 6.8.

Table 6.5: *trans* normal species of 2-PrSH

	*Ab Initio**	Griffiths	Observed
A (MHz)	7831.54	7892.65 (30)	7892.340 (122)
B (MHz)	4319.54	4414.42 (02)	4414.452(80)
C (MHz)	3096.80	3158.03 (01)	3158.069 (80)
D_J (MHz)	0.0013	-	0.0013
D_{JK} (MHz)	0.0027	-	0.0027
D_K (MHz)	0.0024	-	0.0024
d_J (MHz)	0.00037	-	0.00037
d_K (MHz)	0.0028	-	0.0028
Lines Fit	-	12	61
Fit RMS (MHz)	-	0.05	0.165
Max J	-	4	66

Calculated at the B3LYP/6-311++G (d,p) level of theory in Gaussian 09.

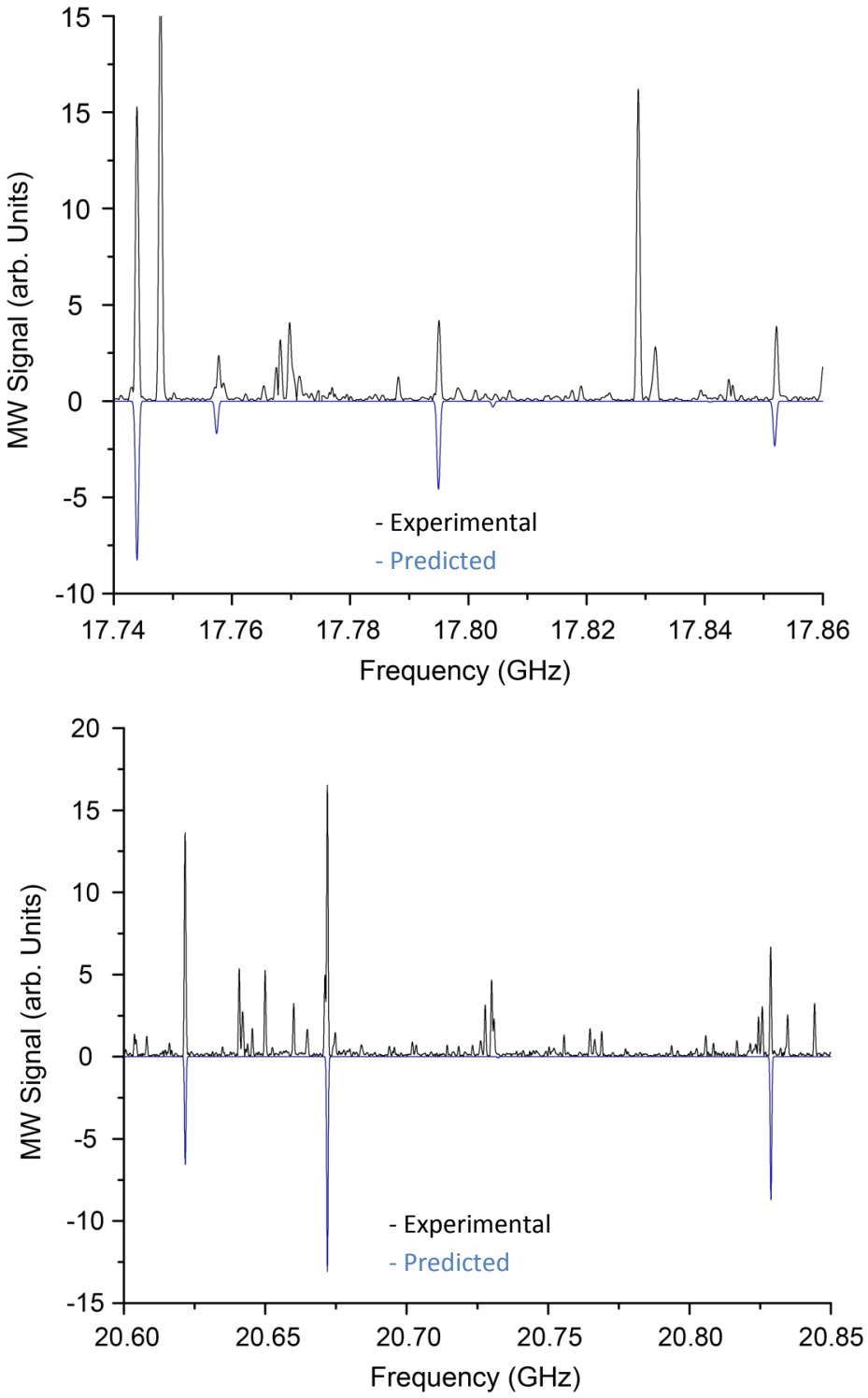

Figure 6.5: Expanded view of the experimental spectrum (black) of 2-PrSH versus simulated data from the experimental *trans* conformer (blue) rotational constants on the negative scale.

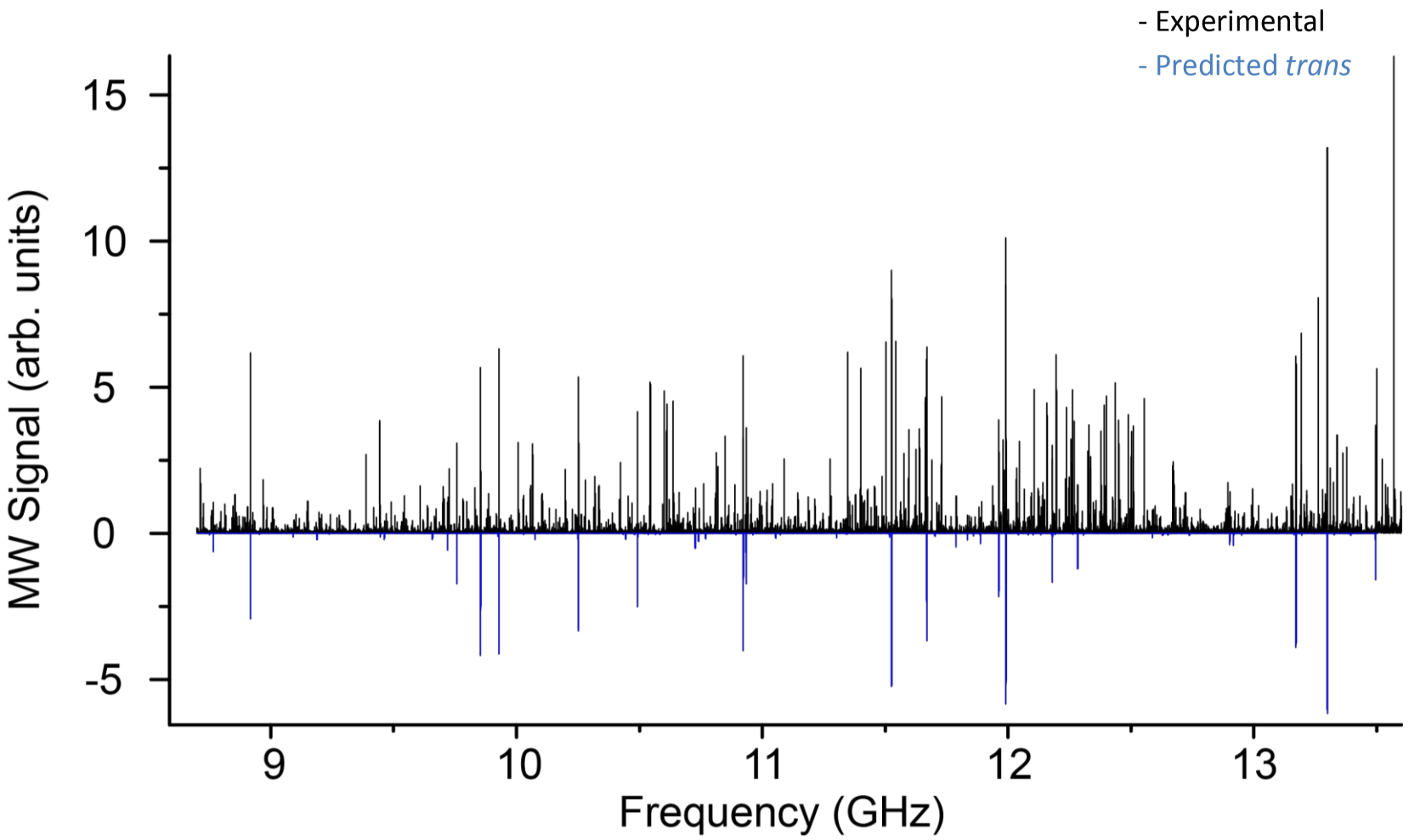

Figure 6.6: Experimental spectrum of 2-PrSH (black) from 8.7 to 13.5 GHz against simulated data from the experimental rotational constants on the negative scale. The predicted *trans* spectrum is simulated in blue.

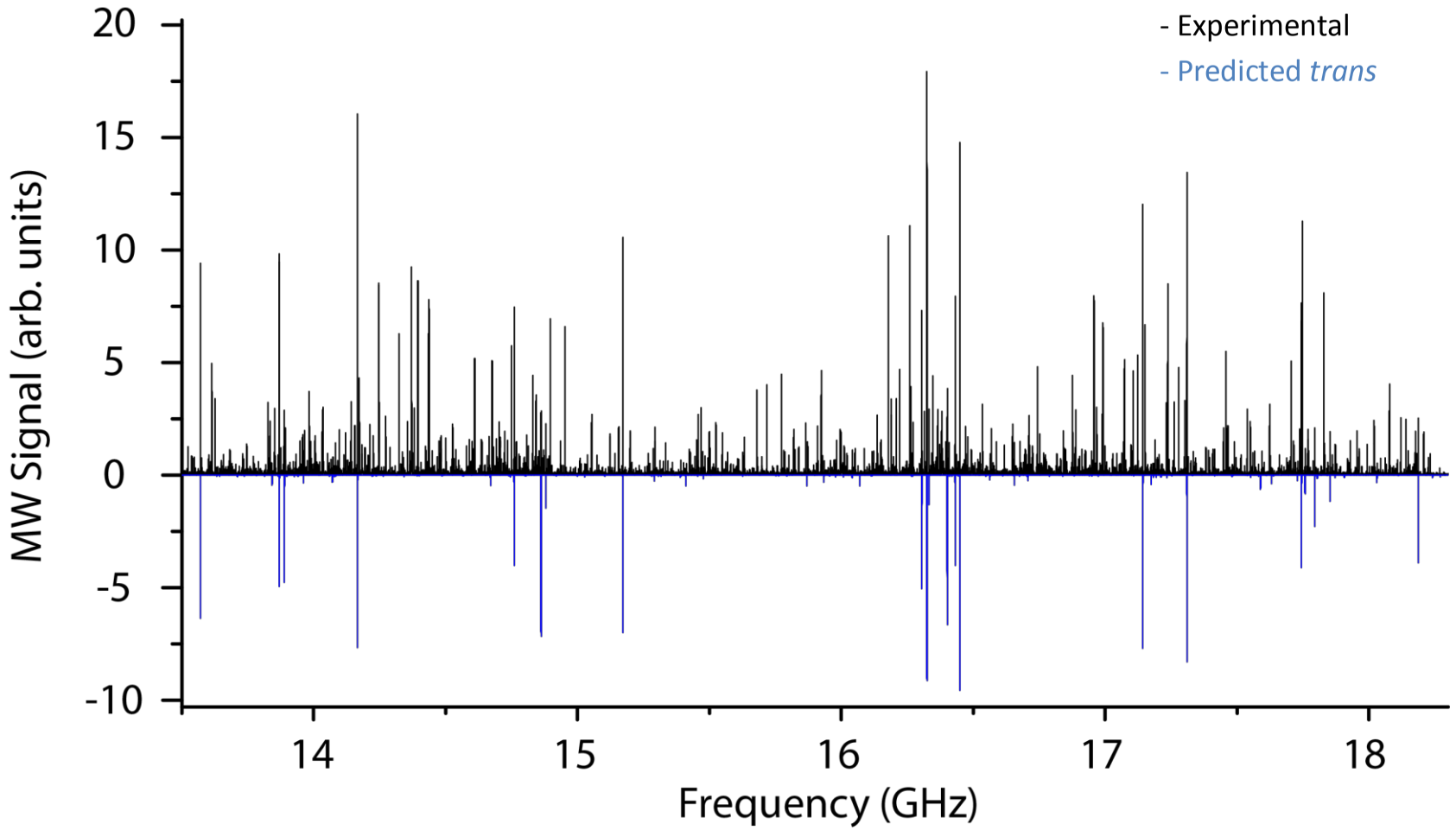

Figure 6.7: Experimental spectrum of 2-PrSH (black) from 13.5 to 18.3 GHz against simulated data from the experimental rotational constants on the negative scale. The predicted *trans* spectrum is simulated in blue.

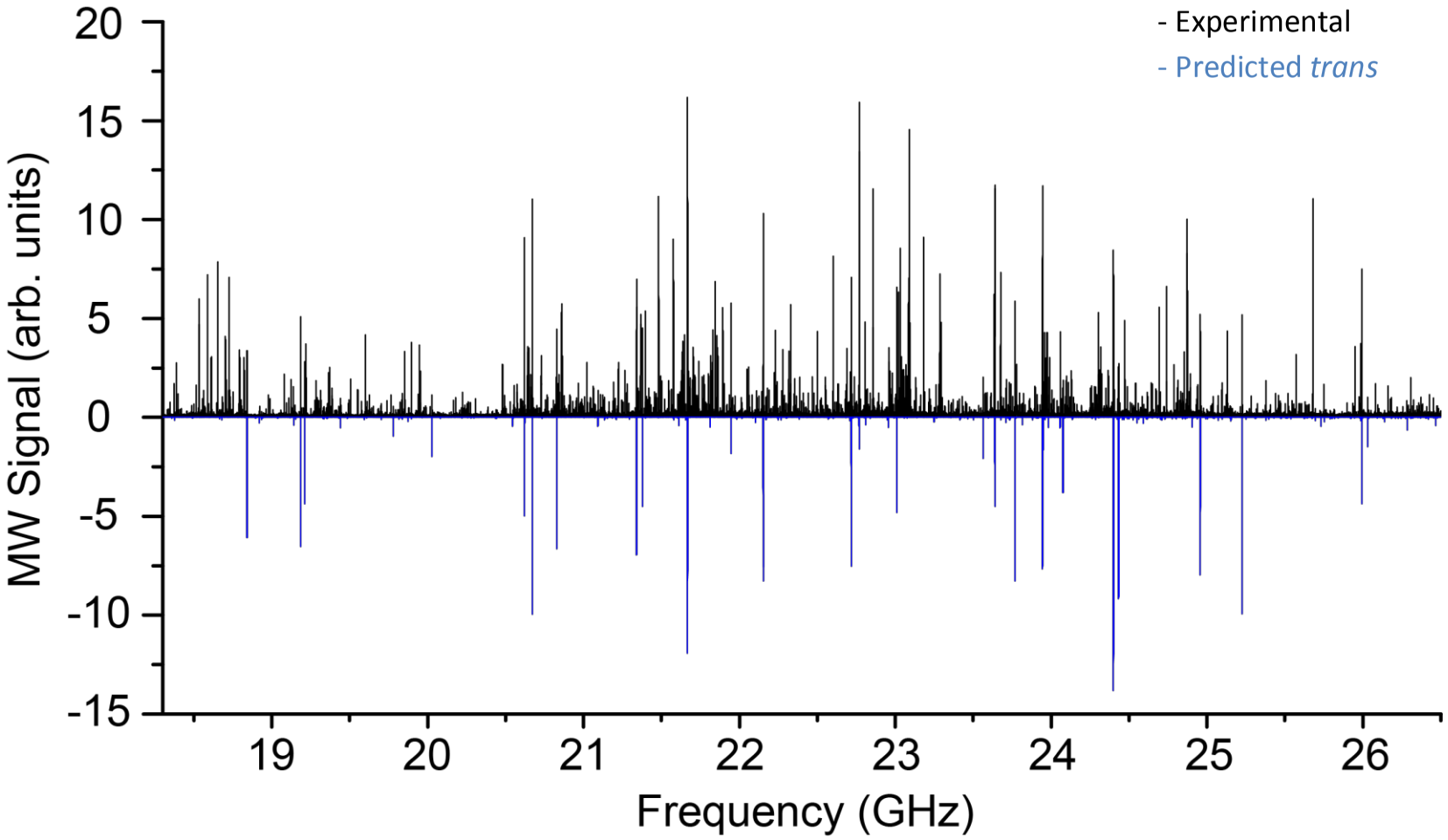

Figure 6.8: Experimental spectrum of 2-PrSH (black) from 18.3 to 26.5GHz against simulated data from the experimental rotational constants on the negative scale. The predicted *trans* spectrum is simulated in

Much work still needs to be done on this spectrum. We will begin testing the Hamiltonian adapted from Hirota *et al*[20]. for the *gauche* conformer and begin fitting that spectrum. There are also several excited vibrational states in appreciable abundance (Table 6.2) that require attention as well. The new digitizer and spectrometer which will no doubt aid future work on this spectrum.

8) Conclusion

The microwave spectra of ethanethiol, 1-propanethiol, and 2-propanethiol were recorded from 8.7-26.5 GHz at ~251 K. All three molecules exhibit splitting in their *gauche* conformers due to thiol tunneling splittings. This splitting was able to be measured in the *g*-EtSH conformer and the TG-1-PrSH conformer, which are very similar in structure and can be fit using the same Hamiltonian. The *gauche* 2-PrSH spectrum could not be adequately modeled with this Hamiltonian and has not been fit to date. However, we have recently adapted the Hamiltonian to more closely resemble the one used by Hirota *et al.*[20] to fit the *gauche* spectrum of 2-propyl alcohol. We are optimistic that this will soon enable us to begin making progress on that spectrum.

None of the alkylthiols discussed in this thesis show splitting in their *trans* spectrum, so these spectra could be fit using the conventional Watson A-Reduced Hamiltonian, but they are not without their own are fitting complications. Because the *gauche* conformer in each molecule is doubly degenerate, transitions from the *gauche* conformer are generally more intense than those arising from the *trans* conformers. The *trans* conformer was able to fit be fit for 2-PrSH, for which it is the most stable structure. However, in *t*-EtSH and TT-1-PrSH are the less stable than their respective *gauche* conformers, so they have an even lower relative abundance. Many of the lower intensity transitions for both molecules could not be fit because they were below the 3:1 signal to noise ratio.

The *t*-EtSH spectrum was able to be fit despite this, but the transitions in the TT-1-PrSH could not be assigned with enough certainty to report an improved fit. This is because 1-PrSH has 6 stable conformers, compared to EtSH's two, and each of those conformers have excited states, as well, some of which are expected to be at a higher relative intensity than the TT-1-PrSH spectrum. The peak intensities in general are expected to be lower for all of the 1-PrSH transitions because the rotational energy is dispersed many different states, resulting in a dense spectrum with many peaks of low intensity in close proximity to one another. Even though several TG-1-PrSH peaks should be that are above the noise level, the potential for false positive identifications is very high.

Many of these difficulties will be trivial for future students due to the imminent hardware upgrades. Currently, one of the greatest roadblocks for fitting is the shortage of strong transitions in our current bandwidth. The new spectrometer's range of 110-170 GHz will significantly ease the challenges. The predicted intensities at those frequencies are much higher than those in our existing frequency range, so transitions that are currently lost to noise will be clearly visible. Finally, the new spectrometer's digitizer will be at least 60 times faster than the one we currently use, so we will be able to take substantially more averages in less time. This should greatly improve the signal-to-noise ratio and allow us to both extend our current fits and to assign the spectra of higher energy conformers and vibrational states.

There is still significant to be done on all of these molecules, but this thesis established a baseline and set the direction for future work. All of the necessary *ab*

initio calculations to generate starting constants for fitting vibrational states have already been performed and are reported in the previous chapters and can be used to guide future work.

References

1.) Wakelam, V., Castests, A., Ceccarelli, C., Herbst, E., Casellim P. "Resetting Chemical Locks of Hot Cores Based on S-Bearing Molecules." *Astronomy &Astrophysics*, **422**, 129 (2004).

2.) Wakelam, V., Castests, A., Ceccarelli, C., Lefloch, B., Caux, E., Pagani, L. "Sulphur-Bearing Species in the Star Forming Region L1689N." *Astronomy &Astrophysics*, **413**, 609 (2004).

3.) "ALMA Basics." https://almascience.nrao.edu/about-alma/alma-basics, Date Accessed 4/29/2013.

4.) Linke, R.A.; Frerking, M. A.; Thaddeus, P.; "Interstellar methyl mercaptan." *Astrophysical Journal* **234**, L139 (1979).

5.) Finneran, I. "The Microwave Spectroscopy of Small Molecules with Methyl Rotors." *Senior Thesis at New College of Florida* (2011).

6.) Bernath, P. F. Spectra of Atoms and Molecules. Oxford Universtiy Press: New York, 159-196 (1995).

7.) Pickett, H. M. "The Fitting and Prediction of Vibration-Rotation Spectra with Spin Interactions." *J. Molec. Spectroscopy,* **148,** 371, (1991).

8.) Brown, G.G., Dian, B.C., Douglas, K.O., Geyer, S.M., Shipman, S.T., Pate, B.H. "A Broadband Fourier Transform Microwave Spectrometer Based on Chirped Pulse Excitation." *Rev. Sci. Insturm.*, **79**, 53103 (2008).

9.) Reinhold, B. Fineran, I.A., Shipman, S.T., "Room Temperature Chirped-Pulse Fourier Transform Microwave Spectroscopy of Anisole." *J. Mol. Spec.*, **270**, 89 (2011).

10.) Phillips, Maria. "Pruning the interstallar weeds…" *Senior Thesis at New College of Florida*, (2013).

11.) Schmidtt, R. E., Quade, C. R. "Microwave spectrum of ethyl mercaptan." *J. Chern. Phys. **62**,* 3864 (1975).

12.) Nakagawa, J., Kuwada, K., Hayashi, M. "Microwave Spectrum, Structure, Dipole Moment and Internal Rotatino of Ethanethiol. II. Gauche Conformer." *Bull. Chem. Soc. Jpn. **49**,* 3420 (1976).

13.) Imanov, L. M.; Qajar, Ch. O.; Abbaoz. A. A.; "Microwave Spectrum of Ethyl Mercaptan." *Phys. Lett. A*, **24**, 485 (1967) .

14.) Kadzar, Ch. O.; Imanov, L. M.; Ch. O.; Abbaoz. A. A.; "Microwave Spectrum and Structrue of Ethylmercaptan Molecule. " *Opt. Spectrosc. (USSR)* **24**, 834 (1968).

15.) Hayashi, M., Kuwada, K., Imaishi, M. "Microwave Spectrum, Structure, Dipole Moment and Internal Rotatino of Ethanethiol. I. Trans Conformer." *Bull. Chem. Soc. Jpn. **47**, 2382* (1974).

16.) Nakagawa, J., Kuwada, K., Hayashi, M. "Internal Rotation in Propyl Mercaptan by Microwave Spectrum." *J. Molec. Spectroscopy, **85**, 327-340* (1981).

17.) Ohashi, O., Ohnishi, M., Taui, A., Sakaizumi,T., Yamaguchi, I."Microwave Spectrum of 1-Propanethiol." *Bull. Chem. Soc. Jpn*. **50**, *1749-1753* (1977).

18.) Griffiths, J. H. “Microwave-Spectrum and Rotational-Conformerism in Isopropyl Mercaptan.” *J. Mol.Spec.,* **56**, *257* (1975).

19.) Meakin, P., Harris, D., Hirota, E. “Barriers to Internal Rotation in Assymmetric Molecules: 3 Fluoropropene.” *J. Phys. Chem.* **52**, 3775 (1979).

20.) Hirota, E. “Internal-Rotation in Isopropyl-Alcohohal Studied by Microwave Spectroscopy.”*J. Phys. Chem.* **83**, 1457 (1979).